

VARIATION OF THE LOCAL MATERIAL
PROPERTIES OF AORTA
Determined through Micro and Nano Indentation

A Thesis
Submitted to
The Temple University Graduate Board

In Partial Fulfillment
Of the Requirements for the Degree
Master of Science
In Engineering

By
Cristina Parenti
January 2010

Dr. Kurosh Darvish
Thesis Advisor
Dept. of Mechanical Engineering
Temple University

Dr. Michael Autieri
Committee Member
School of Medicine
Temple University

Dr. Mohammad Kiani
Committee Member
Dept. of Mechanical Engineering
Temple University

Dr. James Heckman
Committee Member
Dept. of Physiology
Temple University

ABSTRACT

Understanding the aortic wall deformation and failure during traumatic aortic rupture (TAR), which is a leading cause of fatality in motor vehicle accidents is of great concern. The specific objective of the present study is to develop a material model that can describe the multi layer nature of the aortic wall.

Fundamentally, the aortic wall is composed mainly of three layers, *tunica intima*, *media* and *adventitia*, and they are known to have different structures. Understanding the material properties of these layers is essential in order to study the local mechanisms of deformation, force transmission, and failure.

The hypothesis of this study is that the tissue's instantaneous shear modulus grows along the radial direction while moving from the intima toward the adventitia. The higher compliance of the tissue near the intima, which is partly due to the concentration of the smooth muscle cells and partly due to the arrangement of collagen and elastin fibers, can explain the nature of aorta failure which is primarily generated from the inside towards the outer layers.

A combination of micro- and nano-indentation tests were used to measure the local material properties of porcine aorta at the length scales of 160 μm and 40 μm respectively. The material properties of aorta were investigated in the lateral (left) region in several longitudinal locations of the descending aorta and the observed viscoelastic behavior was summarized in the form of instantaneous shear moduli and reduced relaxation functions.

The instantaneous shear modulus was found to generally increase along the radial direction to about 0.6 normalized radial distance and then became almost constant but with higher variability. The reduced relaxation functions were generally independent of the location and test method. Comparing the mechanical results with the histological results obtained through Van-Guisen staining showed that the material properties are partly related to the distribution of smooth muscle cells.

The results of this study can be used to explain the mechanisms of failure in aorta and contribute to improve the computational modeling of aorta's deformation which is valuable in a variety of applications including automotive accidents, endovascular grafts, and angioplasty.

ACKNOWLEDGMENTS

Here I wish to thank the members of my committee and everyone who provided me with their support and help.

Dr. Kurosh Darvish, my adviser and friend, taught me how to combine my scientific passion with the beauty of research. Dr. James Heckman always had good stories and suggestions that prodded me to think and open my mind in fundamental physiology. Dr. Michael Autieri with his lab and Dr. Sheri Kelemen were very kind and gave me the possibility to visualize my biological samples on a microscopic scale. Dr. Mohammad Kiani, the director of my department, helped make everything possible.

The financial support of this research was provided by the National Heart, Lung, and Blood Institute under Grant 5-K25-HL086512-02.

A special note of gratitude goes to Dr. Vallorie Peridier who was always at my side, gave me the opportunity to get into the Masters Degree Program, and helped me complete it from a human and scholastic point of view.

I also have to express my gratitude to all of my colleagues who are now my very good friends; in particular I will mention Sahand Hariri Akbari, Mehdi Shafieian and Kaveh Laksari.

My family gave me the opportunity to move to America and pursue this goal, especially my wonderful mother Joan, my father Nicola, and my aunt Janet.

This whole experience has taught me very much and I will cherish it always.

TABLE OF CONTENTS

ABSTRACT	II
ACKNOWLEDGMENTS	IV
LIST OF TABLES	VII
LIST OF FIGURES	VIII
CHAPTER 1	1
INTRODUCTION	1
HYPOTHESIS	4
SPECIFIC AIMS	5
CHAPTER 2	7
BACKGROUND	7
Material Characterization of Aorta Layers.....	7
Multi-layered models.....	9
CHAPTER 3	11
MATERIALS AND METHODS	11
Spherical Indentation Theory.....	12
Conical Indentation Theory.....	13
Test Setup.....	13
Histology.....	18
CHAPTER 4	23
RESULTS	23
Shear Modulus.....	26
Relaxation Functions.....	35
Statistical analysis.....	39
Distribution of the smooth muscle cells.....	44
CONCLUSIONS	46
CHAPTER 5	48
DISCUSSION	48
BIBLIOGRAPHY	51

APPENDICES	57
APPENDIX A	57
Isthmus region - Anatomy	57
APPENDIX B	59
Sodium Nitroprusside Dihydrate Composition.....	59
APPENDIX C	61
Fundamentals of Viscoelasticity	61
APPENDIX D	63
Van Gieson Staining Protocol.....	63

LIST OF TABLES

Table	Page
Table 3.1: Media Measurements.....	22
Table 4.1 R^2 and slope from curve fitted to viscoelastic coefficients in the radial direction	40
Table 4.2 T tests for viscoelastic coefficients.....	42
Table B.1: Sodium Nitroprusside Calculation.....	54

LIST OF FIGURES

Figure	Page
Figure 1.1: Research plan	3
Figure 1.2: Transverse tear of the aortic wall	4
Figure 3.1: Micro indentation sketch with spherical indenter	12
Figure 3.2: Nano indentation sketch with conical indenter.	13
Figure 3.3: Experimental set up for micro and nano indentation	15
Figure 3.4: Micro indentation on porcine aorta sample.....	15
Figure 3.5: Nano indentation on porcine aorta sample.	16
Figure 3.6: Adventitia Sample 3 (Series 3).....	19
Figure 3.7: Media Sample 3 (Series 3).	20
Figure 3.8: Intima Sample 3 (Series 3).....	21
Figure 3.9: Media Sample 3 (Series 3)	22
Figure 4.1: Tunica intima, media and adventitia (10 X Mag.)	23
Figure 4.2: Vasa Vasorum occupy loose connective tissue (4 X Mag.).....	24
Figure 4.3: Tunica Adventitia (10 X Magnification). Small circle: Nano Indenter tip. Big circle: Micro Indenter tip.....	25

Figure 4.4: Force and displacement history curves from a typical nano-indentation test.	26
Figure 4.5: Heart and first 300 mm of Swine Aorta.	27
Figure 4.6: Differences of Shear Modulus in the Circumferential Direction.	29
Figure 4.7A: Shear Modulus in the Radial Direction (Nano-Indentation).	30
Figure 4.7B: Histogram of the shear modulus in the Radial Direction (Nano-Indentation).	31
Figure 4.8A: Shear Modulus in the Radial Direction (Micro Indentation).....	31
Figure 4.8B: Histogram of the shear modulus in the Radial Direction (Micro Indentation).	32
Figure 4.9A: Shear Modulus with SNP (Lateral Nano Indentation).	33
Figure 4.9B: Histogram of the shear modulus with SNP (Lateral Nano Indentation).	33
Figure 4.10A: Shear Modulus with SNP (Anterior Nano Indentation).	34
Figure 4.10B: Histogram of the shear modulus with SNP (Anterior Nano Indentation).	34
Figure 4.11: Reduced Relaxation Functions from Nano Indentation tests	35
Figure 4.12: Reduced Relaxation Functions from Micro Indentation tests.	36
Figure 4.13: Reduced Relaxation Functions Nano Indentation tests w/SNP.....	37
Figure 4.14: Reduced Relaxation Functions Micro Indentation tests w/SNP.	37
Figure 4.15: Elastic Force Trend	38
Figure 4.16: Viscoelastic Coefficients.	39
Figure 4.17: Viscoelastic Coefficients in the radial direction.....	41
Figure 4.18: Comparison between viscoelastic coefficients from Micro and Nano Indentation.....	42

Figure 4.19: Comparison between viscoelastic coefficients from Micro Indentation and Micro Indentation with SNP	43
Figure 4.20: Aortic wall reconstruction (20X Mag)	44
Figure 4.21A: SMC distribution in the radial direction	45
Figure 4.21B: Histogram of the SMC distribution in the radial direction	45
Figure A.1: Aorta's regions	52
Figure B.1: Sodium Nitroprusside Structural Formula	53
Figure C.1: Three mechanical models of viscoelastic material	55
Figure C.2: Relaxation Function (Force) and Deformation (Displacement)	56

CHAPTER 1

INTRODUCTION

Traumatic aortic rupture (TAR) is a major cause of fatality in motor vehicle crashes. In numbers, 80% of the subjects who experience such trauma die at the scene of the accident 'Parmley LF, Mattingly TW et al'1958. Between the USA and Canada, 7500-8000 victims are counted every year as a result of TAR Richens D, Kotidis K et al. 2003.

TAR is usually caused by automobile crashes but, in general, it can be caused by any different kind of sudden-deceleration injury, including motorcycle collisions, falls from a height, blast injuries, airplane and train crashes or skiing and equestrian accidents. The shearing forces of high speed impacts have been identified as a transverse tear at the isthmus region (Symbas et al. 1973, Burkhart et al. 2001) which is subjected to the greatest strain (Appendix A). In the cases where death does not occur immediately, the vessel is not completely detached and often the symptoms are misleading or unclear. The disrupted aorta can be diagnosed with a chest x-ray image system or an aortography, but there are only a few hours to discover and treat the injured vessel before the lesion becomes fatal. The theories behind TAR are various and the main ones are whiplash effect, intravascular pressure theory, water-hammer effect and osseous pinch mechanism.

The isthmus of aorta lies at the junction between the moveable and fixed regions of aorta. The whiplash theory explains that when a sudden deceleration occurs, the mobility of the ascending aorta and aortic arch, relative to the fixed distal descending aorta, can have an important contributory factor to the rupture.

The intravascular pressure theory attributes the occurrence of TAR to a sudden rise in blood pressure. If the aorta was assumed to be an isotropic cylindrical vessel under pressure, it would rupture axially rather than transversely. The typically observed transverse tears in the aorta could only occur if the transverse strength is more than twice the longitudinal strength. Tensile tests presented by Mohan and Melvin (Mohan D, Melvin JW, 1983)do show that the ultimate tensile strength of the aorta in the transverse direction relative to the longitudinal direction nearly approximates the required rupture ratio of 2:1. The water-hammer effect results when the flow of an incompressible fluid is occluded suddenly, leading to a significant pressure pulse in the aorta. This would be expected to be significantly greater at the aortic arch on account of the curvature reflecting and intensifying the pressure wave. The osseous pinch mechanism is based on normal physiologic motion of the bony thorax, including the rotation of the ribs around their vertebral articulations. Blunt trauma to the chest causes the manubrium, first rib, and the medial clavicles to rotate posteriorly and inferiorly about the axes of the posterior rib articulations. This movement compresses the vascular structures between the anterior osseous elements and the vertebral column; therefore, rupture of the aorta can occur. A better understanding of the physical problem can be achieved by developing mathematical models of TAR.

The internal structure and the material properties of the vessel are determinant factors that need to be implemented in a Finite Element (FE) simulation of TAR during an impact. So in order to fully understand the mechanism of TAR and determine the material properties of the tissue, different studies are being carried out at Temple Biomechanics Laboratory in this regard. The main focus of the present study is to recognize the material properties of aorta determined from micro and nano indentation tests (Figure 1.1). The information acquired by these experiments was then implemented in a computational model of TAR.

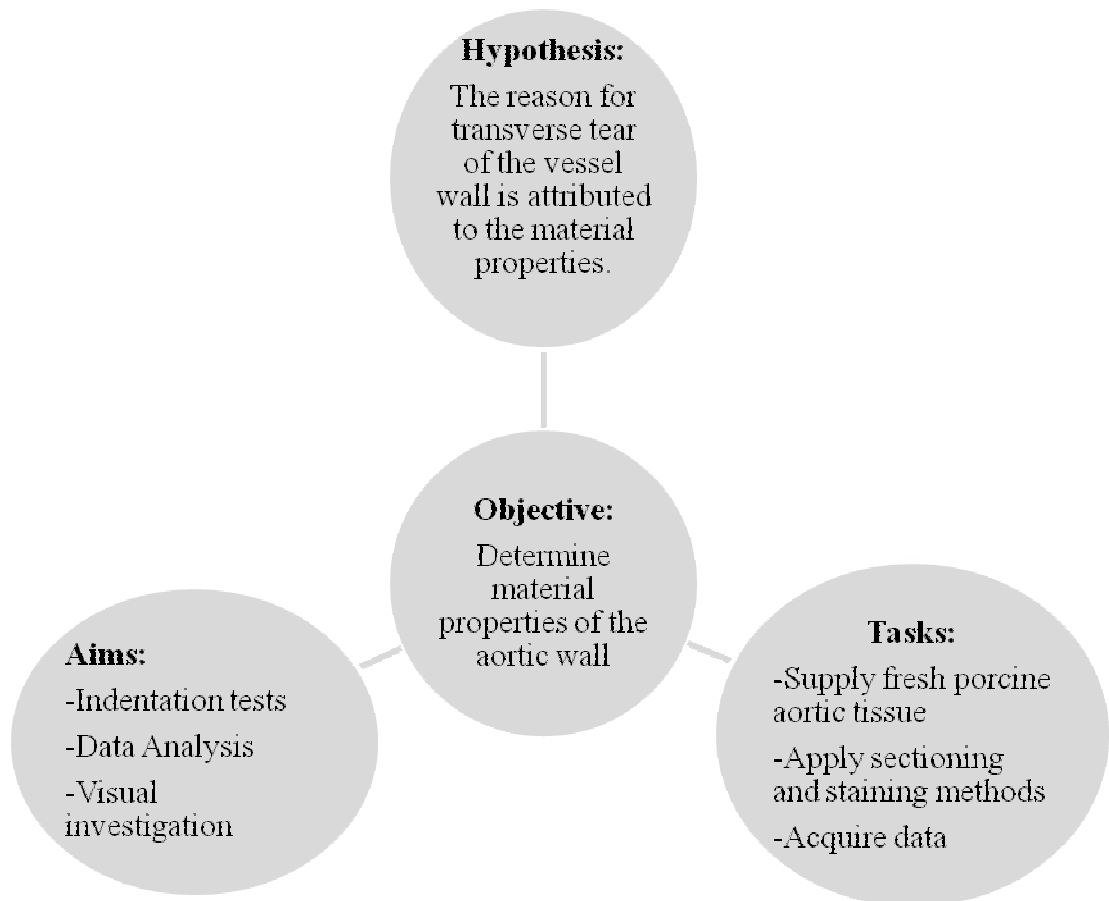


Figure 1.1: Research plan

HYPOTHESIS

The arterial wall material is considered to be a non linear and viscoelastic material of transverse isotropy Cheung JB, Hsiao CC. 1973, and it is known that this kind of biological tissues tends to have a behavior where the stress-strain relationship will change as the loading speed, or better, the strain rate changes (Appendix C).

The hypothesis that drives our study lies in the fact that aorta usually fails in the transverse direction, and therefore the reason why intima fails before the media or adventitia is attributed to the mechanical properties (Figure 1.2).

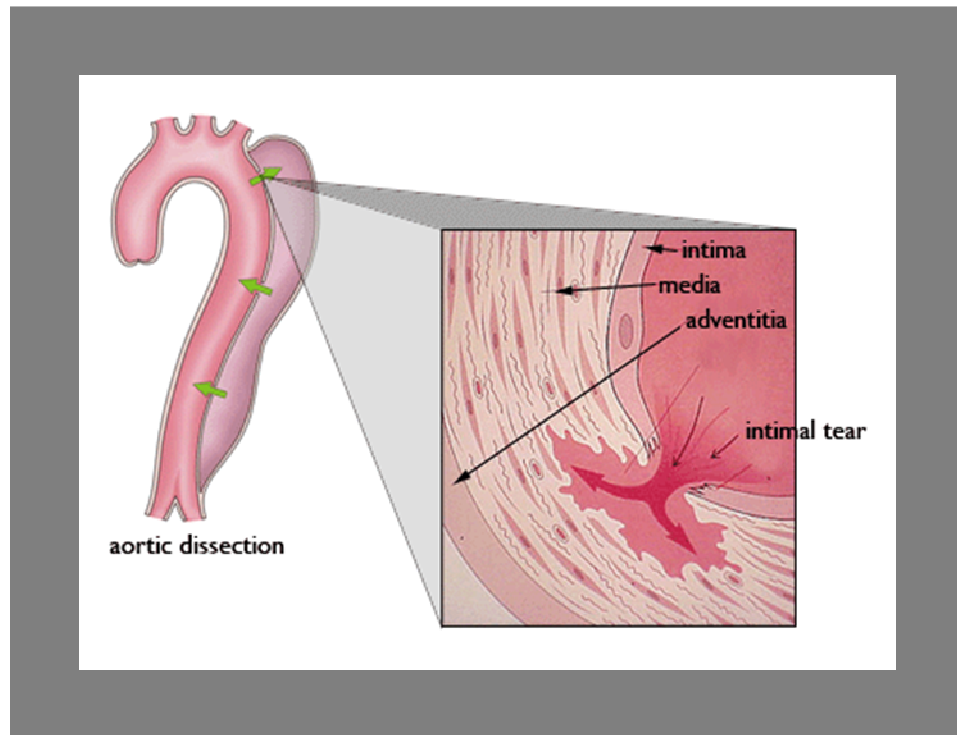


Figure 1.2: Transverse tear of the aortic wall

(www.iradonline.org/images/aorta-layers.gif)

In order to fully understand the mechanism of TAR and determine the material properties of the tissue, different studies are being performed at Temple Biomechanics Laboratory.

In particular, the physical study consists in a quasi static inflation of the vessel, comparing deformation and pressure data; the material properties, instead, were determined by micro and nano indentation tests. The information acquired by these experiments was then implemented in the computational model.

This general prospective shows the complexity of the problem and is all part of multi-year NIH funded projects.

SPECIFIC AIMS

To develop a material model for the aortic wall, there are a number of issues that need to be addressed. First, an accurate representation of the complex aortic material characteristics through constitutive equations is necessary to capture stresses and strains that would lead to aortic rupture during a crash simulation. In addition, material failure criteria are important for predicting the rupture of this vessel (Zhao A 2008).

The specific aims of this study were:

- 1) Indentation Tests: The material properties of the aortic vessel wall were determined by performing micro and nano-indentation tests with the aim of recording force-displacement data acquired in different locations. The samples of intact aorta wall were dissected from surrounding fascia, resulting in the three layers of the specimen that are going to be tested in the radial direction.

- 2) Constitutive Modeling: The force history curves recorded were then analyzed and fitted to the model with the method of least squares; shear modulus was then calculated and characterized for each layer of the aortic wall.

3) Histology: The conformation of the surface that is being explored was then visualized through the process of embedding, staining and light microscopy.

For every layer of the vessel the essential composition is known, but studies have been done on the micro and nanostructure of the aortic medial lamellar unit (O'Connell MK, Murthy S et al'2008) using high technology microscopy imaging. In this project, layer microstructure was identified and explored in order to relate the physical structure to the mechanical properties.

CHAPTER 2

BACKGROUND

Material Characterization of Aorta Layers

Aorta is a distribution vessel which has the function to irrigate cycling blood from the heart to the capillary beds throughout the organism. To operate in this way, the aortic walls have a highly elastic nature and this is demonstrated by the presence of the elastic fibers.

Current material models of aorta assume a homogenous material, whereas aorta is composed of three major layers (Fawcett DW 1994). The innermost layer is the tunica intima. Endothelial cells line the lumen of the aorta within this layer. It also contains loose connective tissue with relatively few fibroblasts, smooth muscle cells, and thin collagen fibers running longitudinally. This layer makes up less than one sixth (Weiss L. 1998) of the vessel wall in humans but is relatively thick compared to other arteries in the body. With increasing age, these cells accumulate lipid, thickening the artery wall. The tunica media is the middle layer consisting of alternating lamellae of elastin and smooth muscle cells. The spaces between the lamellae also contain fine elastic fibers and collagen fibers. The tunica media is the thickest of the aortic wall layers. This layer is responsible for the elastic recoil that maintains blood pressure during diastole. The outermost layer is the tunica adventitia consisting of longitudinally running collagen fibers, thin elastic fibers, and fibroblasts. The tunica adventitia contains small blood

vessels, known as vasa vasorum, and nerves to nourish and innervate the outer half of the aortic wall (Dellman H 1981).

The adventitia's main responsibility is to stop excessive dilatation in order to prevent permanent deformation.

The injury mechanism of TAR is still unknown since it is difficult to replicate and evaluate such ruptures experimentally (Cavanaugh J M, Walilko T J et al.), although the hypotheses have been proposed for TAR, such as relative motion between heart and ascending aorta, intravascular pressure, the water-hammer effect and osseous pinch. The primary site of TAR in 75-85% of all cases is reported at the isthmus which is a transition region between a relatively mobile heart and a relatively fixed descending aorta (Kalita P. 2008).

As stated, knowledge of the material properties of the aortic wall is fundamental for understanding aortic rupture mechanisms. Mechanical experiments on excised human aorta tissue showed that the tissue is highly rate sensitive and fails at large strains, approximately from 10% to 90% (Mohan D, Melvin JW. 1982). One factor contributing to the large variability observed in the material properties of different aortas is age: specimens dissected from older subjects exhibit a stiffer response and fail at smaller strains. More recently, Darvish et al. (Darvish K. , Lobovsky L. et al. 2004) performed dynamic biaxial tests with large strain on porcine and human tissues and proposed a hyper-viscoelastic model that can mathematically describe both the previous uniaxial data and the new biaxial data. Previous aorta wall failure data suggests that strain is a better measure of tissue failure than stress. For previous material characterizations, aorta was assumed to be uniform along its thickness. However, since aorta wall has three distinct layers (Fawcett DW 1994), an understanding of the material properties of these layers is essential in order to study the local mechanism of failure as a crack propagates through the aorta wall. To our knowledge, no data has been reported with regard to the material

properties of individual layers of aorta wall. Many instances of partial aortic rupture occur (about 10% to 20%) in which the outermost layer of aorta does not rupture and the patient's chance of survival is significantly increased (Fattori R. , Celletti F. et al. 1994). Considering the mechanism of partial aortic rupture and the risk of fatality of TAR, knowledge of the material properties of aorta wall layers is vitally important to the survival of trauma victims.

Multi-layered models

The mechanical characteristics of the blood vessels mentioned previously can be summarized in constitutive equations that represent each and every vessel and the material properties need to be determined from experimental data. For example, the aorta stress and the strain data can be obtained using vessel inflation, and axial and biaxial stretching. The stiffness of the vessel can be obtained by using micro and nano indentation tests. In vivo studies are also performed for aorta material characterization using two different types of methods; one is invasive, such as intravascular ultrasound and angiography. The second method is noninvasive and uses processes such as magnetic resonance imaging, and ultrasound. These methods can be used to study blood pressure, changes in vessel geometry, state of disease, and responses to outside stimuli, such as exercise and pharmacological agents. The results of the above mentioned experiments on the vessels revealed that the vessels can be characterized as nonlinear, anisotropic, and viscoelastic materials (Vito R.P. , Dixon S.A 2003).

Another issue is heterogeneity, i.e., the vessels cannot be treated as if their walls have a uniform structure. Furthermore, depending on the experiment type, vessels can be treated as compressible (when studying fluid exchanges within the walls) or incompressible (when the fluid exchange can be neglected). But despite the long list of attributes, a constitutive equation can only account for a certain combination of these

parameters. As previously mentioned, the vascular wall is constructed of cells, elastin, and collagen, the location of which varies for each of the layers. The orientation of elastin and collagen is load dependant, which changes the overall material property as load is being applied. The complication for the modeling conditions is that even though the vessels have not always been treated as homogeneous on a microscopic level, their exact structure is too complicated to replicate. To solve this problem, the vascular model is simplified to a two- or three-layered cross section.

For passive or unstimulated aorta, Vito and Dixon (Vito R.P. , Dixon S.A 2003), using a Lagrange multiplier approach, and based on biaxial data, suggested the following forms of strain energy function (W) for media:

$$W_{media} = \frac{c}{2} (\exp[c_1(C_{11} - 1) + c_2(C_{22} - 1) + c_3(C_{33} - 1)] - 1) \quad (1)$$

which is anisotropic. C_{11} , C_{22} and C_{33} represent the strain coefficients and c , c_1 , c_2 , c_3 are the material constants. In contrast, they suggested an isotropic model for adventitia.

$$W_{adv} = \frac{\beta}{2\alpha} (\exp[\alpha(I_c - 3)] - 1) \quad (2)$$

Were α and β are again material constants and I_c is the first invariant of the strain tensor.

$$I_c = C_{11} + C_{22} + C_{33} \quad (3)$$

Yet, this model has some caveats:

- it is not clear whether the media and adventitia were truly tested in isolation, for it is stated that the aortic specimens were split roughly in two;
- The assumption of isotropy of the adventitia was not well supported.

CHAPTER 3

MATERIALS AND METHODS

In the present study, the mechanical properties of the vessel are going to be determined assuming the vessel to be locally homogeneous and quasi-linearly viscoelastic for small deformations. The experimental setup is designed to perform indentation testing, specifically micro indentation with a spherical indenter and subsequently nano indentation with conical indenter for further analysis. During the indentation tests, the displacement and force were recorded. The force history of the indenter $P(t)$ was characterized using a quasi-linear viscoelastic (QLV) model:

$$P(t) = \int_0^t G(t-\tau) \frac{\partial P^e(h)}{\partial h} \frac{\partial h}{\partial \tau} d\tau \quad (4)$$

in which $P^e(h)$ is the instantaneous elastic force that can generally be a nonlinear function of the indentation depth h . $G(t)$ is the reduced relaxation function which was assumed to be a Prony series:

$$G(t) = G_\infty + \sum_{i=1}^4 G_i \exp(-\beta_i t) \quad (5)$$

with G_i and β_i representing the amplitudes and decay rates of relaxation respectively. Four decay rates were chosen to capture the decays that occurred on the orders of magnitude of 0.01, 0.1, 1.0 and 10.0 s.

Spherical Indentation Theory

The relationship between the elastic force P^e and h for the spherical indenter (0.2 mm diameter) was assumed to have the same form as the linear elastic solution for a spherical indenter:

$$P^e = \frac{8\mu}{3(1-\nu)} \sqrt{\frac{D}{2}} h^{3/2} \quad (6)$$

in which P^e is the total elastic force, D is the diameter of the indenter, h is the depth of penetration, μ is the shear modulus, and ν is the Poisson's ratio assumed to be 0.49 (Sneddon, I. N. 1965).

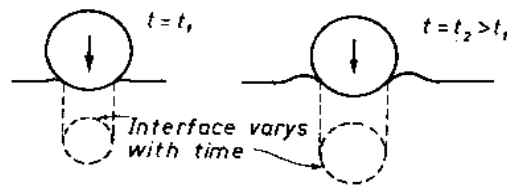


Figure 3.1: Micro indentation sketch with spherical indenter (Findley *et al.*, 1976)

The correspondence principle that is used to analyze the indentation data requires the contact area to be constant during the indentation test. For the spherical indenter (non-

flat indenters in general) contact surface changes over time, as shown in Figure 3.1. When the indentation depth is much smaller than the radius of the indenter, it is assumed that the error due to variable contact surface is negligible.

Conical Indentation Theory

The total load necessary to cause a penetration h for a conical indenter can be written as (Sneddon, I. N. 1965):

$$P^e = \frac{4\mu \cot(\beta)}{\pi(1-\nu)} h^2 \quad (7)$$

where β is the cone angle with the horizontal axis (Figure 3.2).

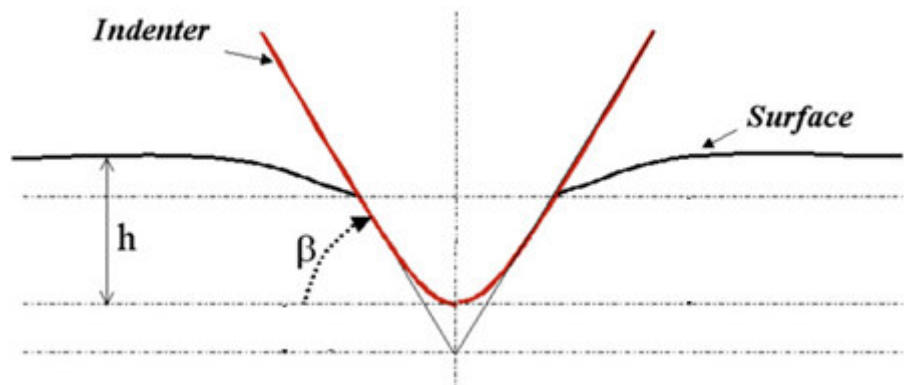


Figure 3.2: Nano indentation sketch with conical indenter.

Test Setup

An apparatus has been assembled to perform micro and nano indentation test together (Figure. 3.3) and it consists of the following elements: two force transducers for each indenter (Aurora Scientific, Ontario, Canada, Model 406A, and Transducer

Technique, CA, GSO series), a 300x Zoom Stereo Microscope (Olympus SZX7), a Z-axis nano-positioner (MCL, WI, Model Nano-Z100) having 60 μm range of motion combined with a horizontal piezo micro-positioner (PI, MA, model M-663.4 PX). The images below (Figure 3.4) show the tip of the spherical indenter used for micro indentation tests: the sample moves in the negative y direction (Nano-Z) for indentation and in the x direction (Piezo-Motor) for the next test. The diameter of the sphere is 0.2 mm. The calibration of the two indentation instruments was checked and verified by testing 20% homogeneous gelatin samples.

The samples utilized in this study consist of fresh swine heart and aorta segments that were purchased from a local slaughterhouse, then immediately submerged in PBS solution and stored in an ice filled cooler while transported to the Biomechanics Laboratory. The aortic arches and descending aortas were cleaned from the surrounding excessive tissue and ring shaped samples were cut in the transverse direction. The tissues were kept in PBS and refrigerated before testing.

In the first series of tests, two transverse sections of fresh (2 to 3 hours postmortem) porcine thoracic aorta were tested for micro indentation in two different locations that were 90° apart. In each location two to four points were selected for indentation (0.3 mm apart) moving in the radial direction. The indenter displacement was a ramp and hold with 60 μm depth, 30 ms ramp time, and 20 s hold time. For this series of micro indentation tests, the initial location of indentation was the posterior side. In subsequent test series, the aortic vessel was also marked before sectioning with various water proof ink colors and all the locations (medial/lateral/anterior/posterior) for each sample were determined.

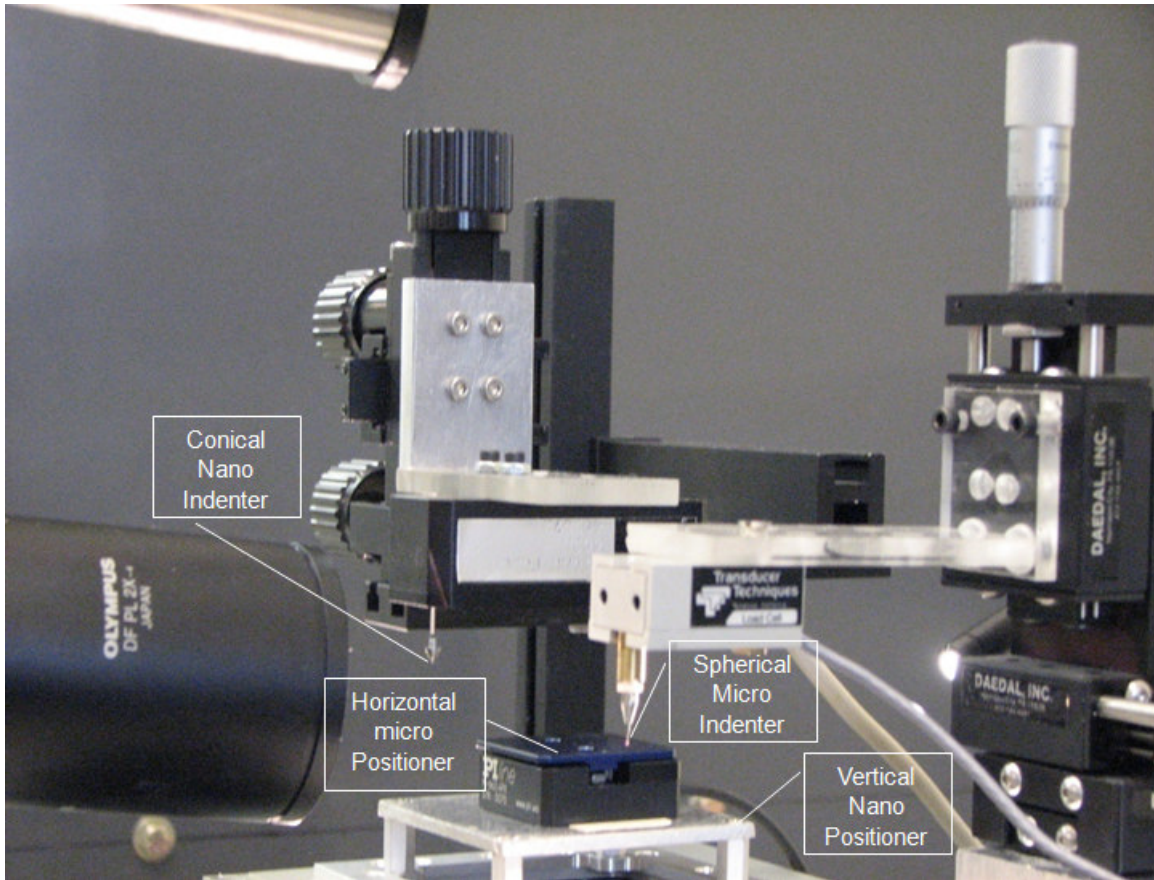


Figure 3.3: Experimental setup for micro and nano indentation

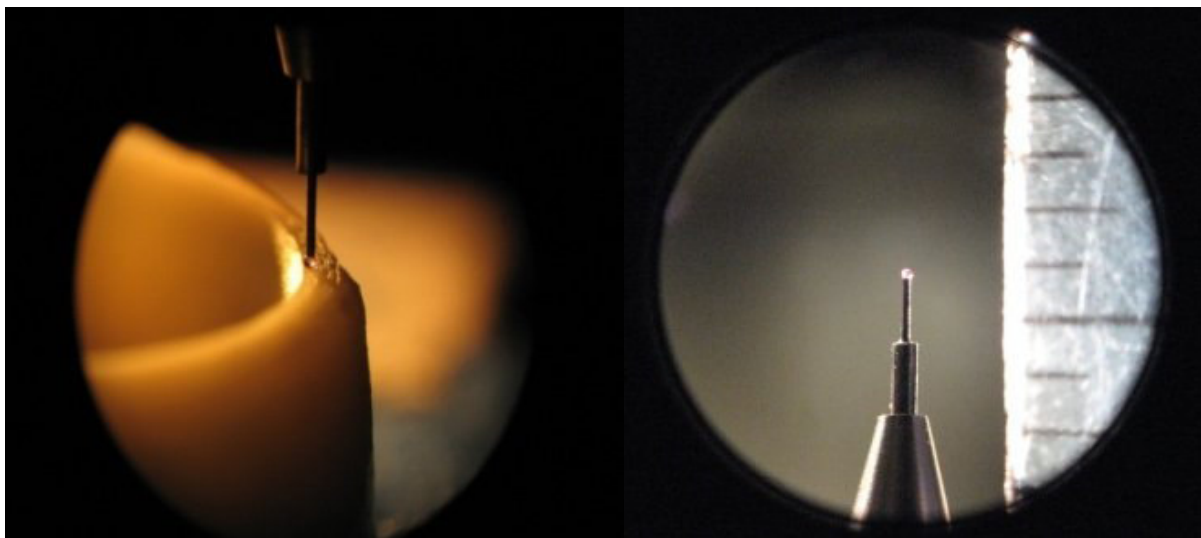
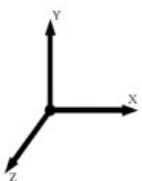


Figure 3.4: Micro indentation on porcine aorta sample.



A limitation of the micro indentation study is that due to the size of the indenter, aggregate material properties were measured at approximately 300 μm length scale. Nano indentation tests were then conducted to yield a better understanding of the individual microstructural properties (collagen, elastin, and cell layers) that are needed to investigate crack propagation through the layers (Figure 3.5).

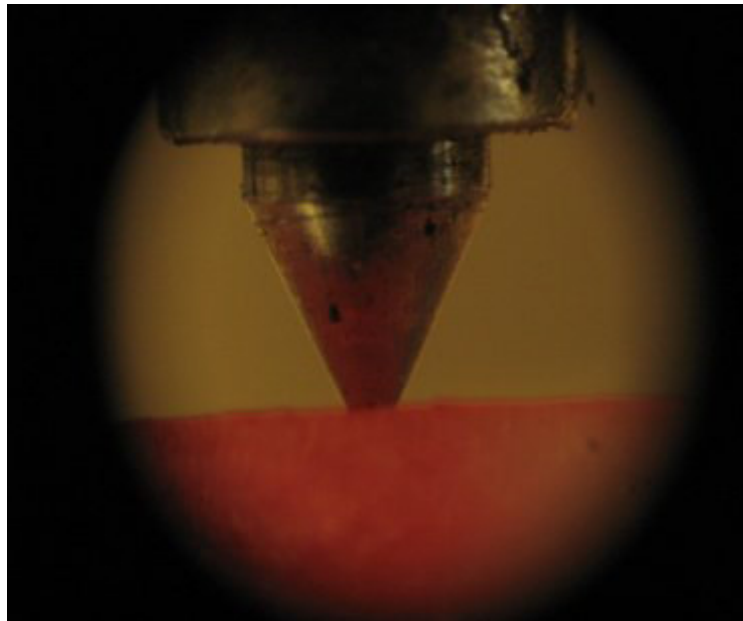


Figure 3.5: Nano indentation on porcine aorta sample.

In the second series of tests, six samples of porcine aorta were tested with a conical indenter (62.5° angle), recording force and displacement measurements. Starting from 50 mm under the arch, six rings of fresh aorta samples (less than 6 hours post-mortem) were dissected to be tested.

Nano indentation tests were performed in the longitudinal direction moving along the radial direction starting from the inner layer (*tunica intima*) toward the outer layer (*tunica adventitia*). The samples reported in this study were on the lateral (left) side with

respect to the chest orientation. The distance between one indentation test and the next one was chosen to be 0.2 mm based on the dimensions of the nano-indenter (300 nm tip radius) and the thickness of aorta (about 2 mm). The indenter displacement was a ramp and hold with 30 μm depth, 10 ms ramp time, and 10 s hold time.

A third series of tests was conducted to perform micro and nano indentation test on the same samples; three segments were investigated on both lateral sides with respect to the heart together with the anterior and posterior locations. Fresh samples (3 hours post mortem) were cut this time 70 mm under the aortic arch and the segments were close to a cm in height.

For further investigation a fourth series of tests was conducted performing mainly nano indentation, but this time the tissue was exposed to smooth muscle cell relaxation process; the samples were soaked in a Sodium Nitroprusside Dihydrate solution (Appendix B), 10^{-5}M concentration previous to indentation testing and the segments were cut starting 90 mm under the aortic arch.

Because of the longitudinal variability of the samples chosen, a fifth series of test was conducted. In this case, two different aortas were purchased at the same time and 5 hours post-mortem the micro and nano indentation testing started. Ring samples for both the vessels were cut at 40-50-80 and 90 mm under the arch; these specific longitudinal points were chosen to evaluate and compare the shear modulus values and trends in respect to the previous results.

It is known that the tunica intima is the most vulnerable layer in aortic failure (Zhao,Aihong 2008) and usually this is where the tear in TAR originates. This study attempts to explain this phenomenon based on the variability in the material properties throughout the layers.

Histology

For the third series of tests, samples were collected in the same region to perform also histology analysis; specifically, the rings of aorta chosen were the ones adjacent to the ones used for micro and nano indentation. The purpose of this additional study was to investigate in detail the surface that was getting indented. As said previously, the aortic wall is not a homogeneous material; therefore, when indenting it is very important to know what is being tested.

The intima of large elastic arteries is composed of endothelial cells, the basal lamina (~80nm thick) and the sub-endothelial layer composed of collagenous bundles, elastic fibrils, smooth muscle cells and some fibroblast (Fung YC. 1993).

The method chosen to visualize the components of the aortic wall (collagen, nuclei, smooth muscle cells etc.) was the Van-Gieson staining (Appendix D).

Samples were kept in 70% ethanol previous to the embedding procedure; once the three samples were embedded with paraffin, it was possible to cut 30 micron thick slices with the microtone. The tissue was then placed on the slides for further investigation. A total of nine slides were chosen to be stained with the Van Gieson Solution; pictures from this study are relevant for size, location and geometry of the components within the aortic wall.

The following pictures obtained with the Van Gieson method show parts of the tunica adventitia, media and intima of a sample #3 (thickness 1.18 mm) third series. The abundance of Fibroblast and Collagen Matrix (stain red-pink) in the Adventitia is shown in Figure 3.6, (40X Mag) while the wavy yellow lines of elastic lamina and numerous nuclei belonging to the smooth muscle cells in the Media are evident in Figure 3.7.(30 X Mag.). Figure 3.8 shows more concentration of the collagen bundles.

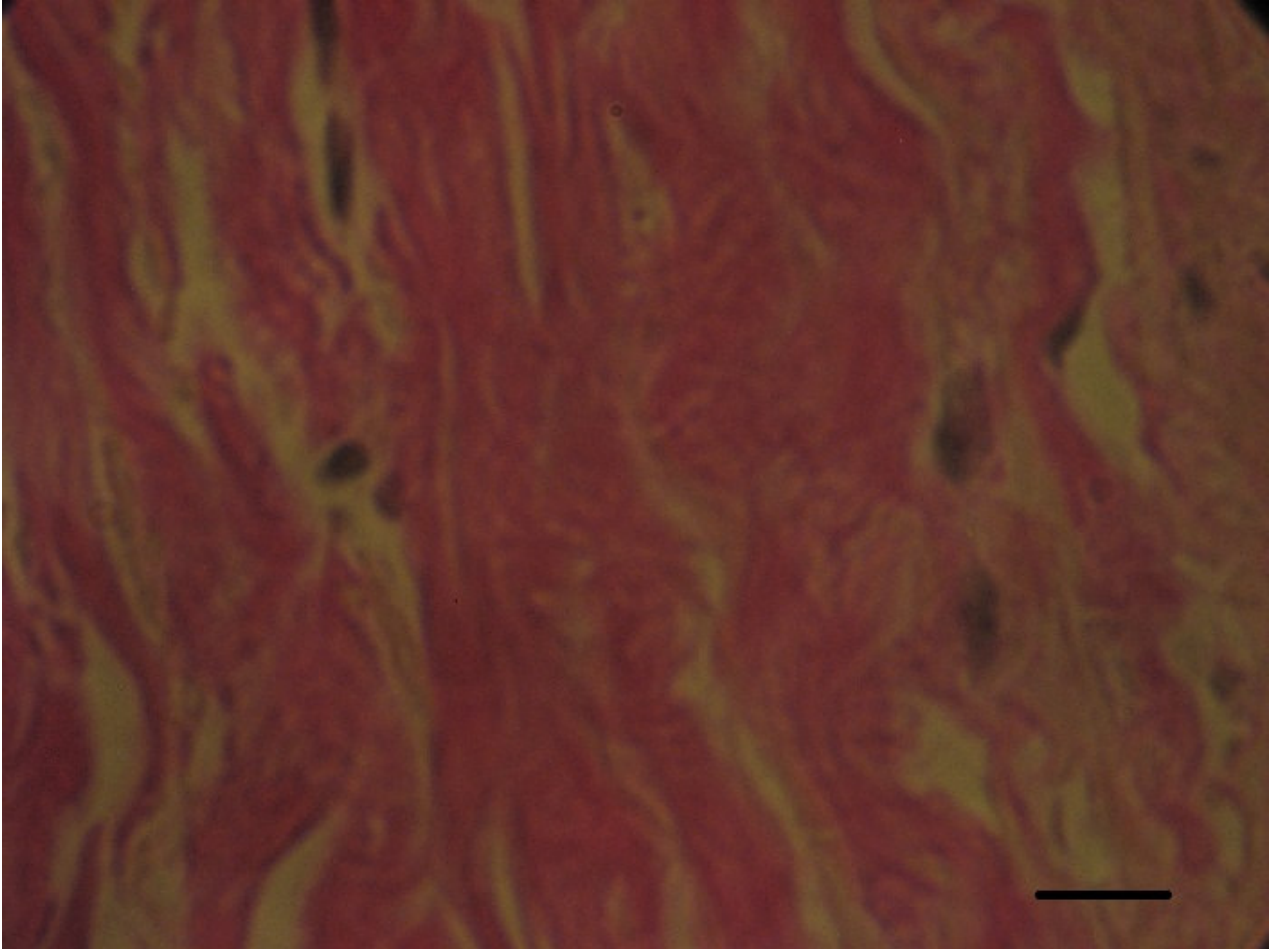


Figure 3.6: Adventitia Sample 3 (Series 3).

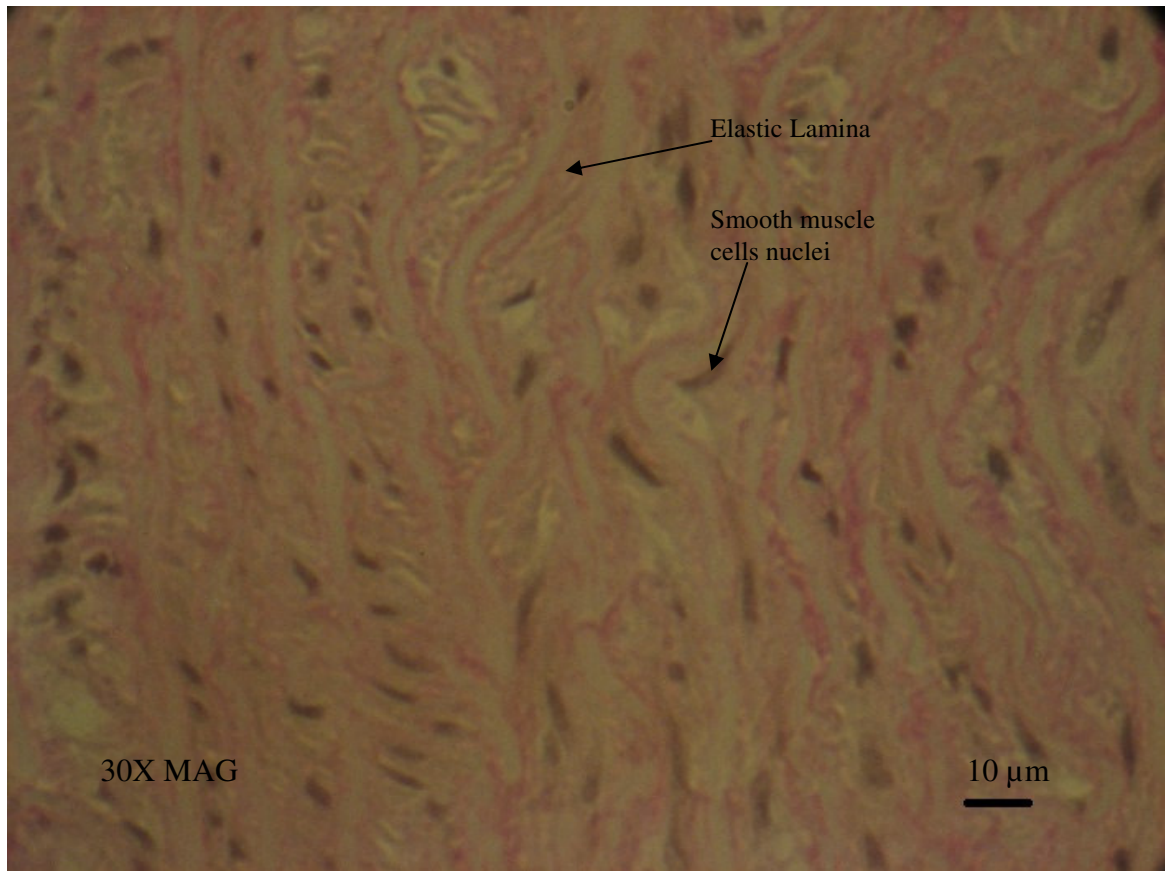


Figure 3.7: Media Sample 3 (Series 3).

The areas measured for the smooth muscle cell nuclei are in the order of $20 \mu\text{m}^2$. The number and thickness of elastic laminae vary with age (Netter's Essential Histology, William et al.). Smooth muscle cells in the media synthesize and secrete elastic fibers as well as some collagen and other elements; collagen confers tensile strength to arterial walls, and elastic fibers impart distensibility, which allows passive recoil under pressure.

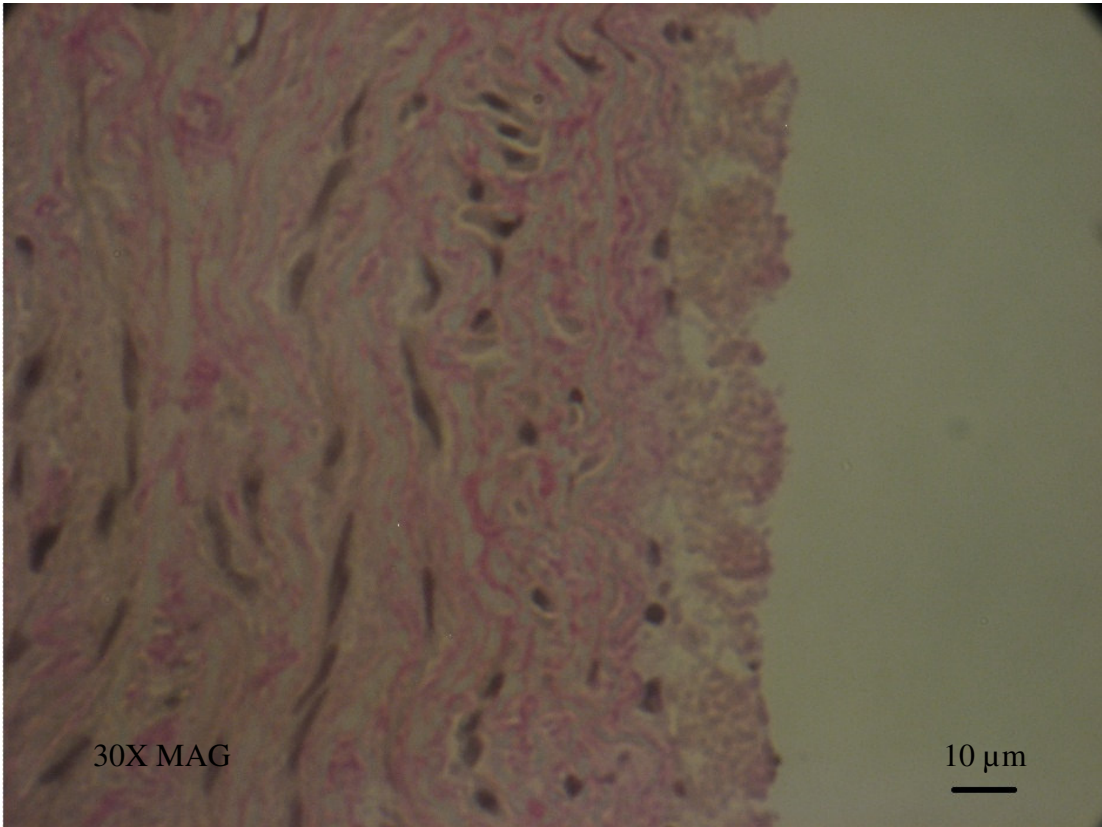


Figure 3.8: Intima Sample 3 (Series 3).

Figure 3.9 shows the technique utilized to measure the number of visible smooth muscle cells nuclei in a 50.25 mm² Area of tunica media. Six samples were analyzed from different specimens and results are described in the following chapter.

A table is presented below to summarize the number and type of tests conducted throughout the entire research (Table 3.1)

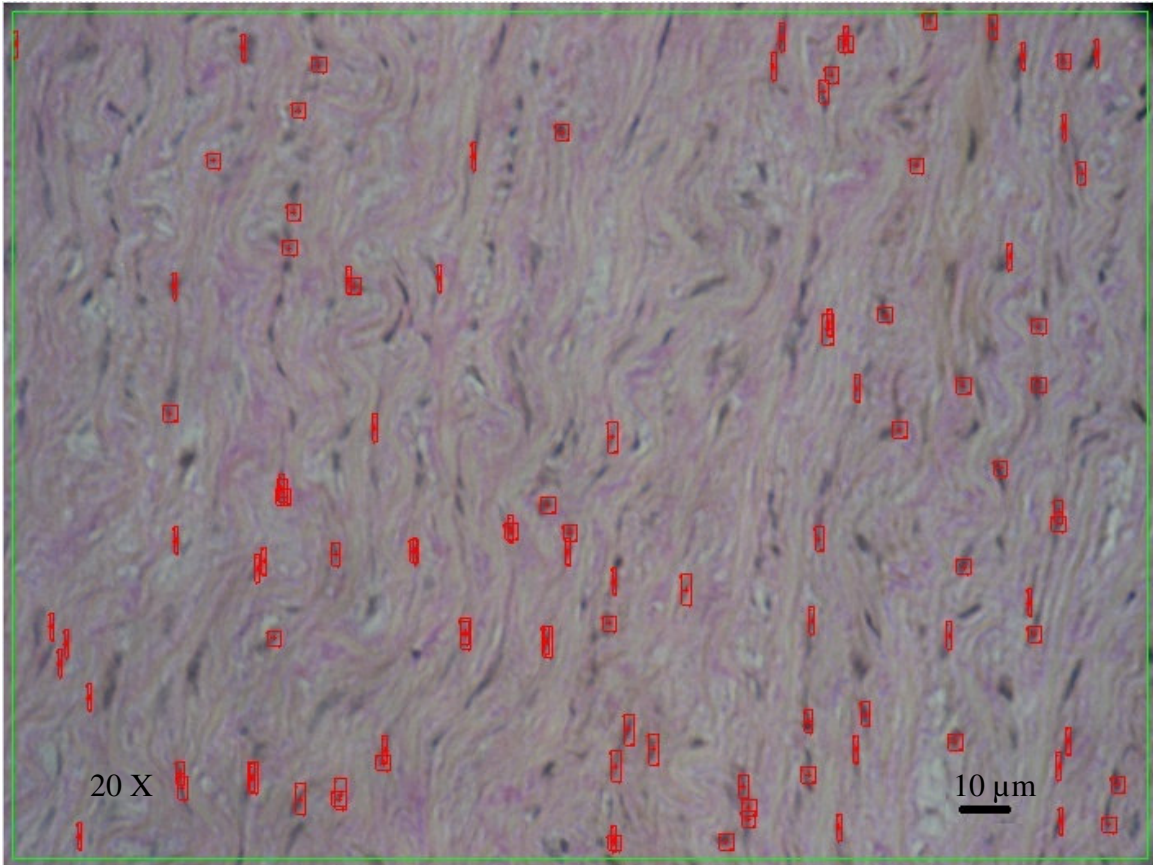


Figure 3.9: Media Sample 3 (Series 3).

	<i>Aorta</i>	<i>Date</i>	<i># Samples</i>	<i>Test type</i>	<i>SNP</i>
1	Aorta	01/22/09	2	Micro	No
2	Aorta	03/04/09	3	Nano	No
3	Aorta	04/07/09	3	Micro+Nano	No
4	Aorta	06/30/09	3+1	Nano	Yes+No
5	Aorta	07/28/09	3+1	Micro+Nano	No+Yes
6	Aorta	07/28/09	2	Micro+Nano	No

Table 3.1: Summary of Tests

CHAPTER 4

RESULTS

The histological photographs, as expected, showed that elastic arteries are composed of a thin, sub endothelial layer of loose connective tissue with a few fibroblasts and rare smooth muscle cells in the intima layer. The relatively thick tunica media has spirally arranged smooth muscle cells, thick collagen fibers and many elastin fibers. The tunica adventitia blends with the surrounding connective tissue so it is hard to determine the specific thickness (Figure 4.1/4.2).

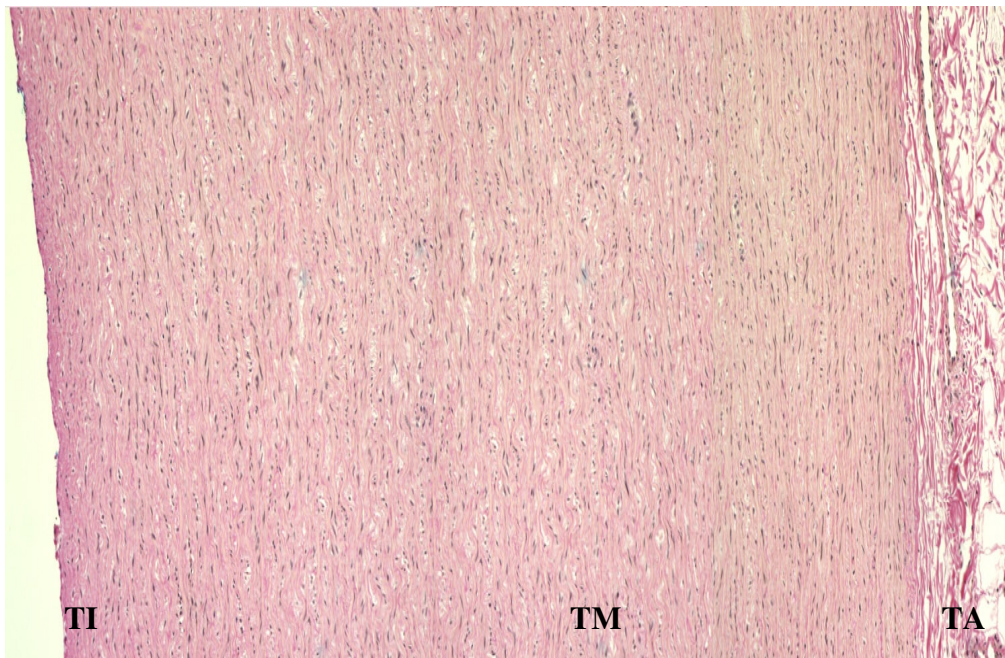


Figure 4.1: Tunica intima, media and adventitia (10 X Mag.).

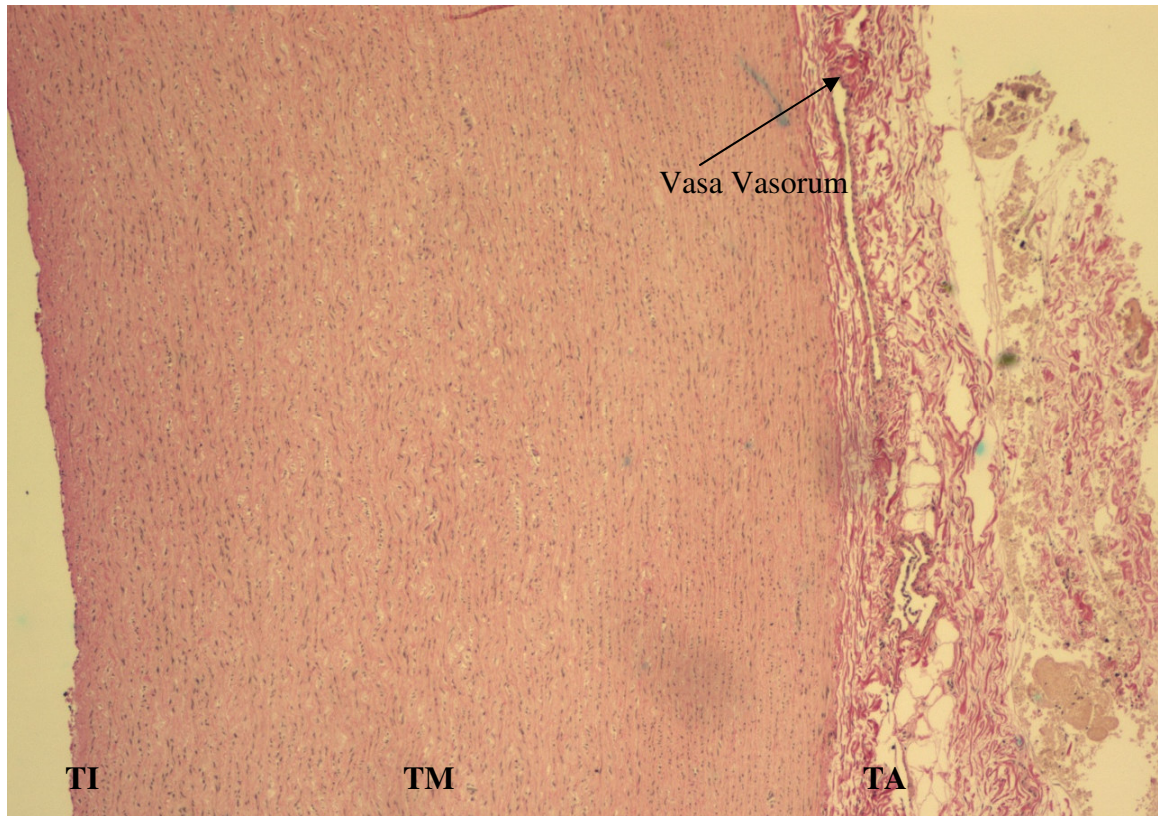


Figure 4.2: Vasa Vasorum occupy loose connective tissue (4 X Mag.).

From the Van Gieson staining process it was possible to identify the smooth muscle cells nuclei and to visualize collagen and elastin fibers. Nine samples were cut 30 micron thick from the embedded blocks for slide preparation and staining. Multiple sections from media were then photographed at different magnifications (10X, 20X, 30X, 40X) and six of them were analyzed through Vision Assistant software to identify the concentration of smooth muscle cell nuclei in the tunica media. Results show that there are approximately 3 smooth muscle cells nuclei per millimeter square. The media can be 0.5 to 2 mm thick and the elastic laminae are 2-3 μm thick and they are fenestrated with a few connecting bundles of elastic fibers in between. The elongated, branched aortic smooth muscle cells are attached to the elastic laminae by types I, II, and IV collagen and are embedded in ground substance (Netter's Essential Histology, William et Al.)

Another consideration that arises through histology analysis is to compare the size of the indenters with the components of the aortic wall. For a 40 μm displacement the circumferential area calculated for the conical and spherical indenters is respectively 1850 μm^2 and 20000 μm^2 . This indicates that the nano indenter area covers approximately 100 times the size of the smooth muscle cell nuclei ($\sim 20\mu\text{m}^2$), while the micro indenter covers a greater area that might include different components (Figure 4.3).

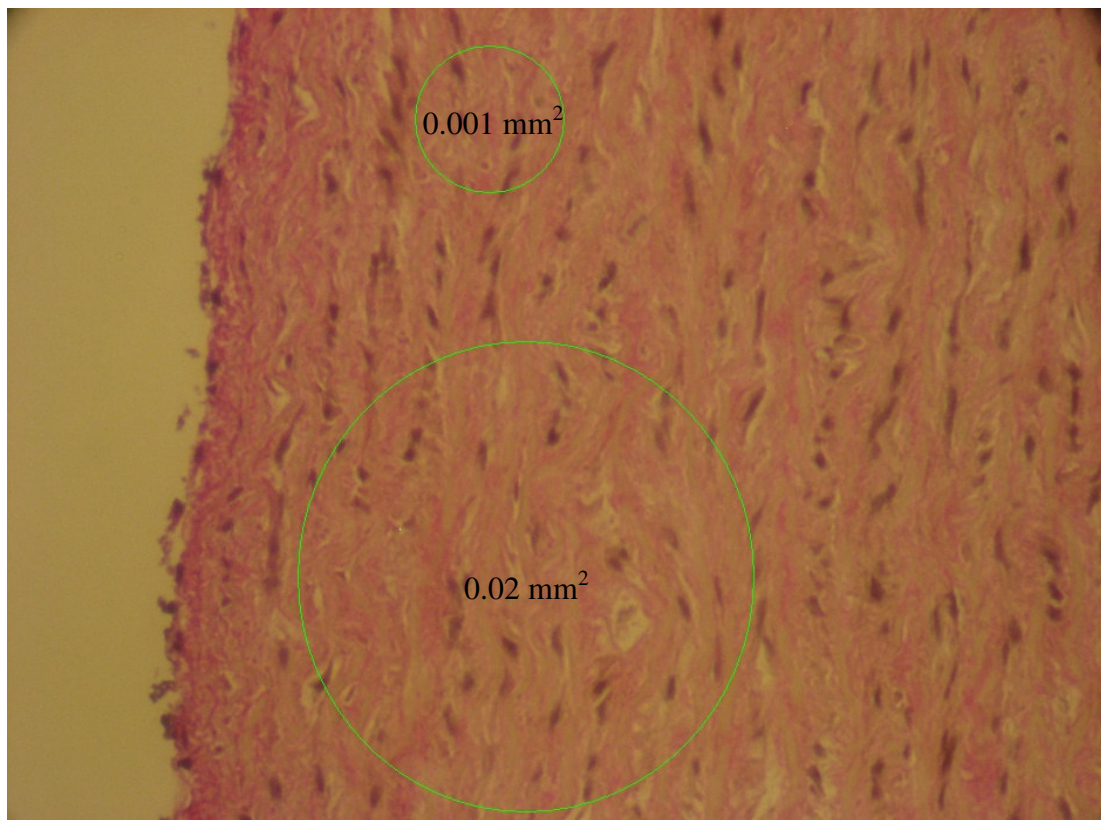


Figure 4.3: Tunica Adventitia (10 X Magnification). Small circle: Nano Indenter tip. Big circle: Micro Indenter tip.

Shear Modulus

From both micro and nano indentation tests the QLV material properties (Equations. 5, 6 and 7) were determined by fitting the models to the experimental force history curves with the method of least squares.

The values of aortic shear modulus derived from the instantaneous force data (Figure 4.4) indicate that the material shear modulus is in the range of 150 to 450 kPa.

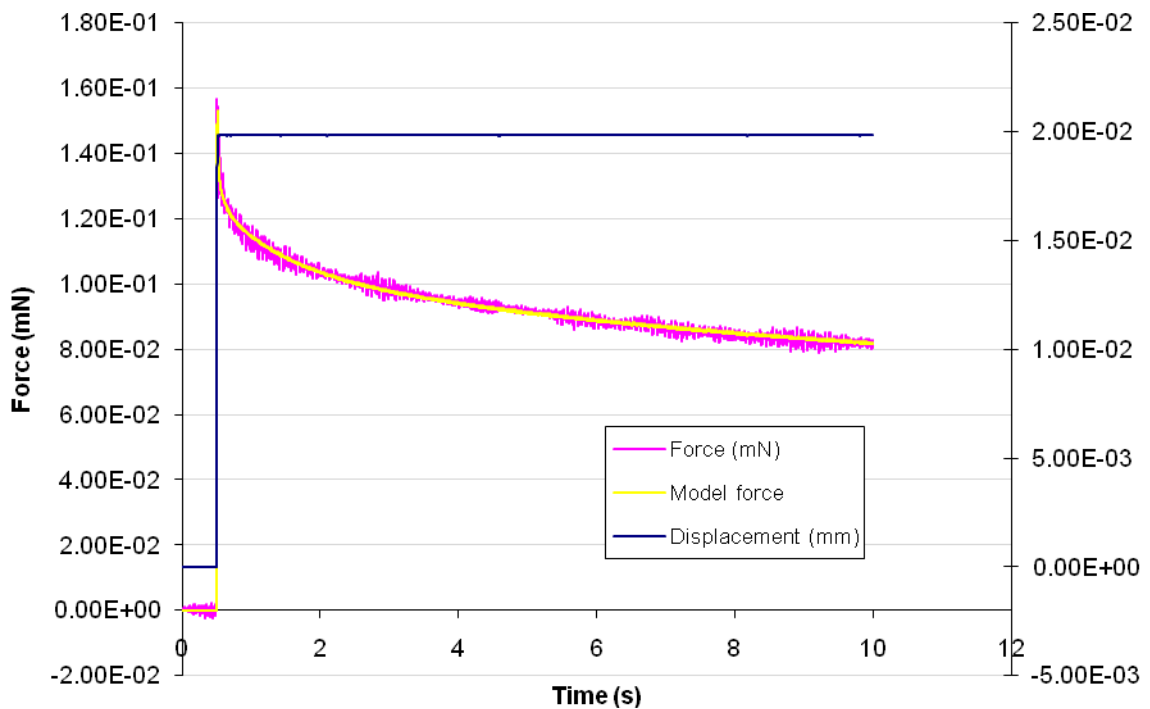


Figure 4.4: Force and displacement history curves from a typical nano-indentation test.

Preliminary results showed that the range of 150 to 450 kPa could be applied for 60% of the aorta's thickness (going from the inner layer towards the outer layer), while the remaining 40% needed further investigation. Micro and nano indentation was then

performed throughout the entire thickness and results show that the shear modulus in the neighborhood of the adventitia can increase up to 600 kPa.

The reason for this variability found in the shear modulus can be attributed to the variability in the microstructural components of the aorta wall including smooth muscle cells, collagen fibers, and elastic lamellae.

When indenting with the spherical tip of 0.2 mm diameter, the regions affected were greater than the ones indented by the conical nano tip. Collagen and elastin fibers of the porcine aorta might get in the way of the conical indenter, requiring a greater force to penetrate between them compared to the force needed for the spherical one to bend the fibers.

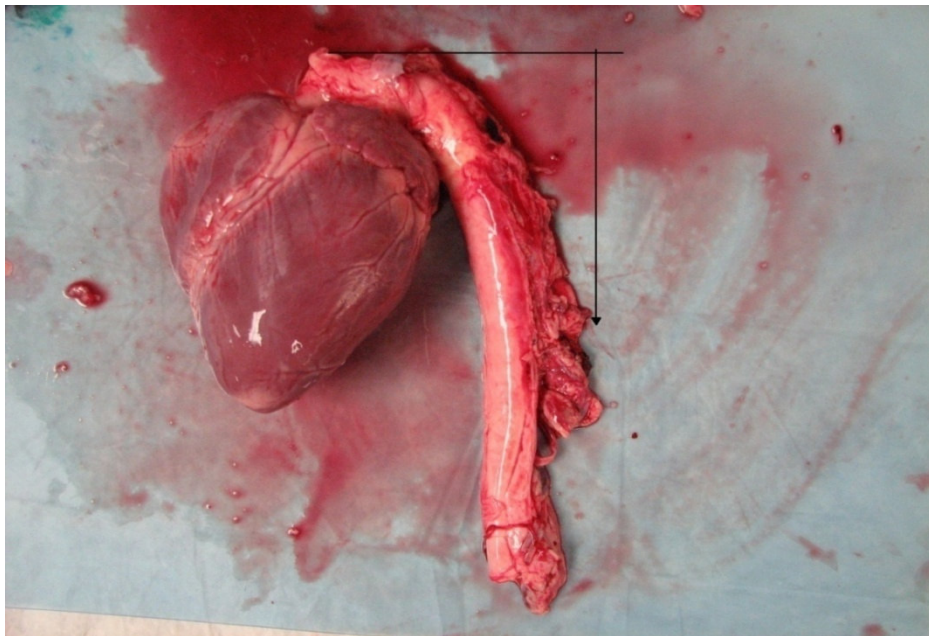


Figure 4.5: Heart and first 300 mm of Swine Aorta.

Although this range found is relatively vast, it can still be considered consistent with previous work found in literature, e.g., the rat aorta (183 ± 25 kPa), the porcine right

coronary artery (210 ± 46.5 kPa), and the porcine left anterior descending artery (231 ± 55.1 kPa) (Matsumoto,Takeo 2004).

The majority of the tests analyzed and plotted for this research study were performed along the lateral sides of the aortas in order to make comparisons between results. Differences were found for the shear modulus values while moving in the circumferential direction. One example is plotted in Figure 4.6, were three nano indentation tests performed in approximately the same radial location ($r=0.5$) are compared. Results show how, according to the circumferential and longitudinal position, the stiffness of the vessel varies. More data is need to make any conclusions on this issue however, in literature this observation is well supported. G. A. Holzapel writes in the *European Journal of Mechanics* that the concentration and arrangement of constituent elements and the associated mechanical properties of arterial walls may depend significantly on the species and the topographical site [see, for example, the early work by Roy (1880–82)]. The ratio of collagen to elastin in the aorta increases away from the heart (Wolinsky and Glagov, 1967) and the corresponding tensile responses of circumferential and longitudinal specimens vary along the aortic tree (Bergel, 1961a, 1961b; Learoyd and Taylor, 1966; Tanaka and Fung, 1974, among many others).

Sample 1, 2 and 3 have been taken respectively from 70, 82 and 95 mm under the aortic arch and it is noticeable how Sample 1 shows the greatest variability of the shear modulus in the different circumferential locations (Anterior, Posterior, Medial and Lateral). Sample 2 follows the trend and seems to be less stiff, while Sample 3 shows greater homogeneity.

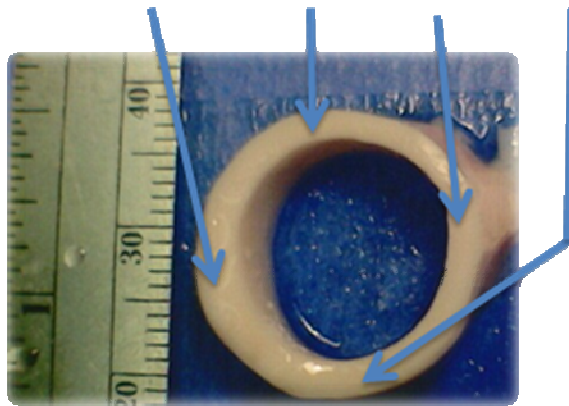
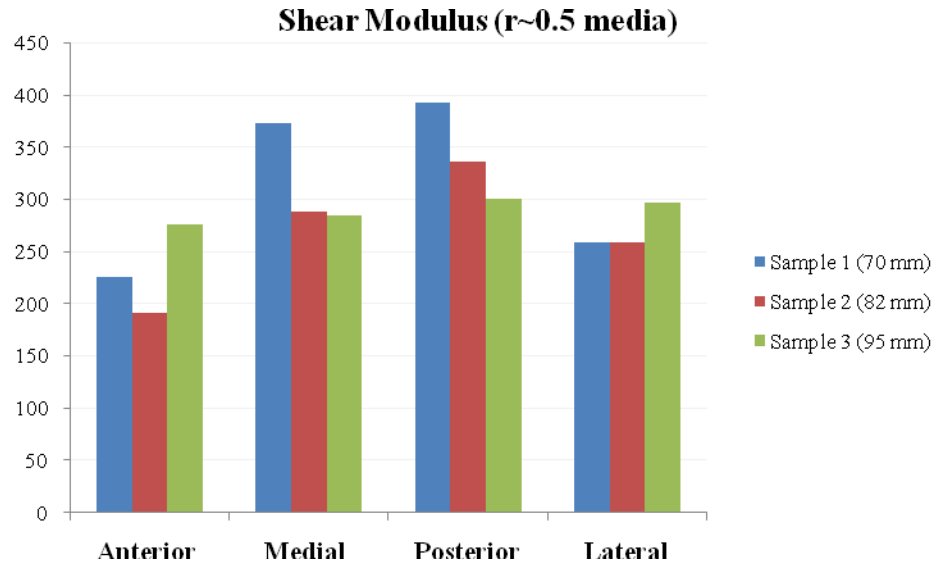


Figure 4.6: Differences of Shear Modulus in the Circumferential Direction.

The six series of test performed and analyzed for the lateral side of porcine aortic vessel show that the stiffness of the aortic wall generally increases while moving toward the adventitia. Some tests show a greater slope than other ones, and some (particularly from micro indentation) show some homogeneity. Figure 4.7 contains shear modulus results obtained from Nano Indentation test performed on seven aorta samples in the radial direction. In particular, results from four different Aortas are reported (Aorta 2-Aorta 3-Aorta 5-aorta 6) and the particular longitudinal location is also included (50-70-75-80-82-90 mm) for every sample. The shear modulus values here have an increasing

trend while moving from intima toward the adventitia from nano indentation testing; once 60% of the radial thickness is reached, results show some variability dependent upon the material constituents.

The normalized distance along x-axis represents the thickness of the vessel scaled from 0 to 1 where the distance of the specific indented points to the edge of the inner layer that was acquired with image processing, was divided by the thickness of the vessel at the particular locations. Micro indentation results are shown in Figure 4.8.

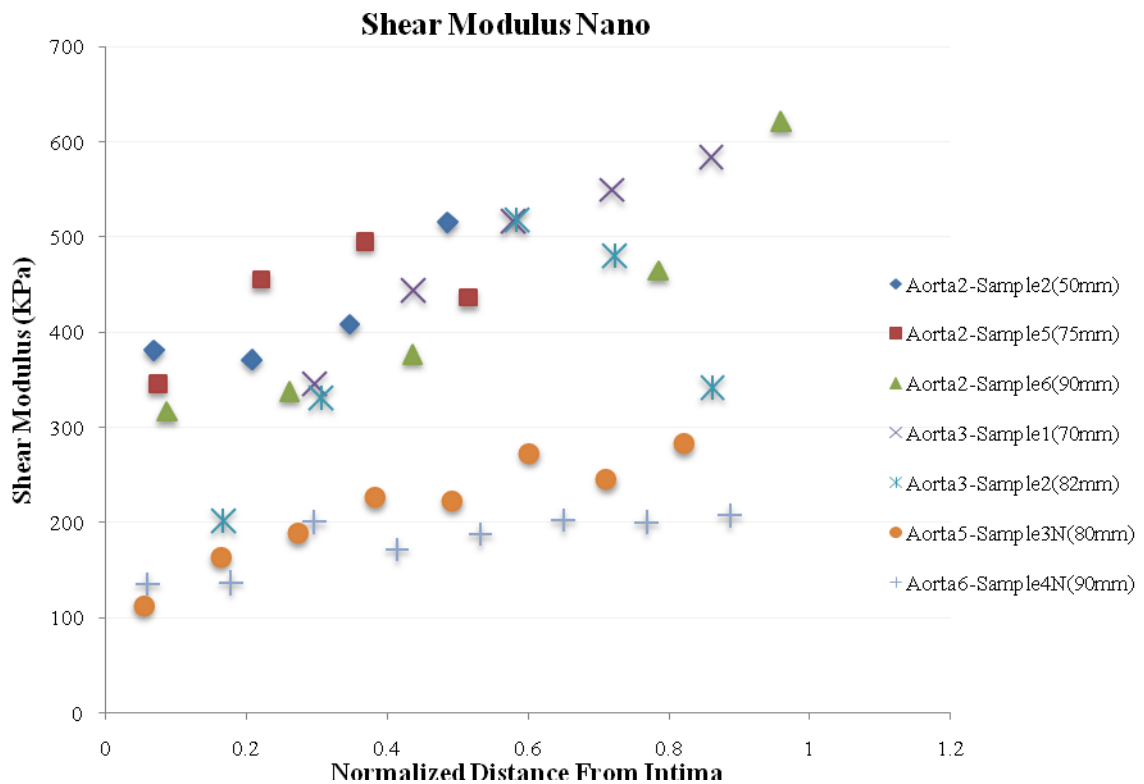


Figure 4.7A: Shear Modulus in the Radial Direction (Nano-Indentation).

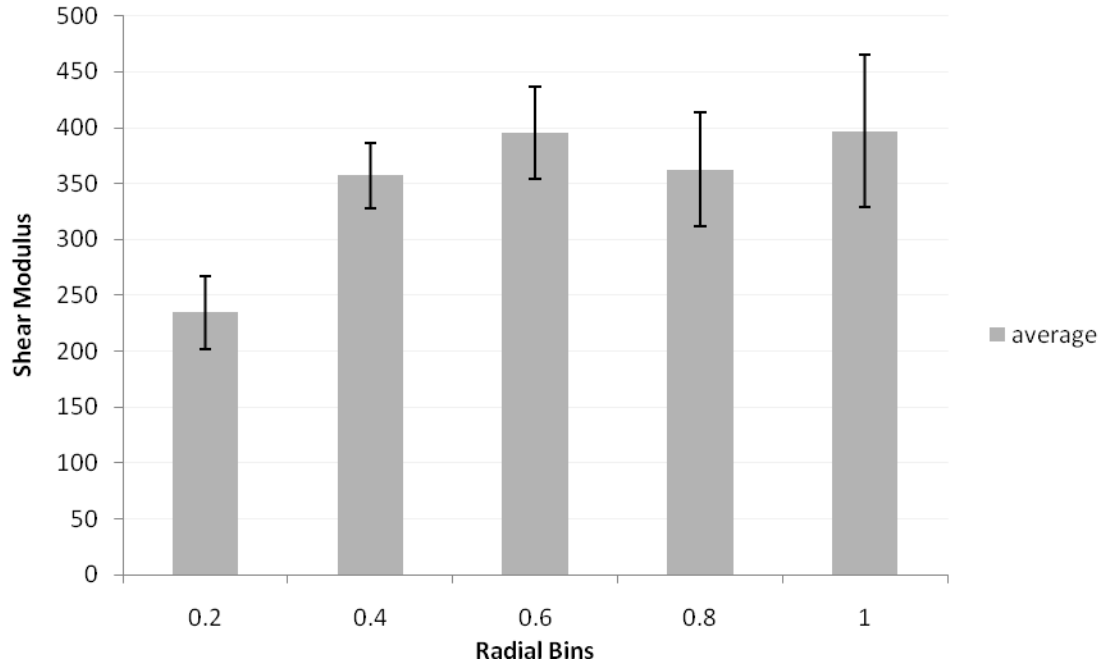


Figure 4.7B: Histogram of the shear modulus in the Radial Direction (Nano-Indentation).

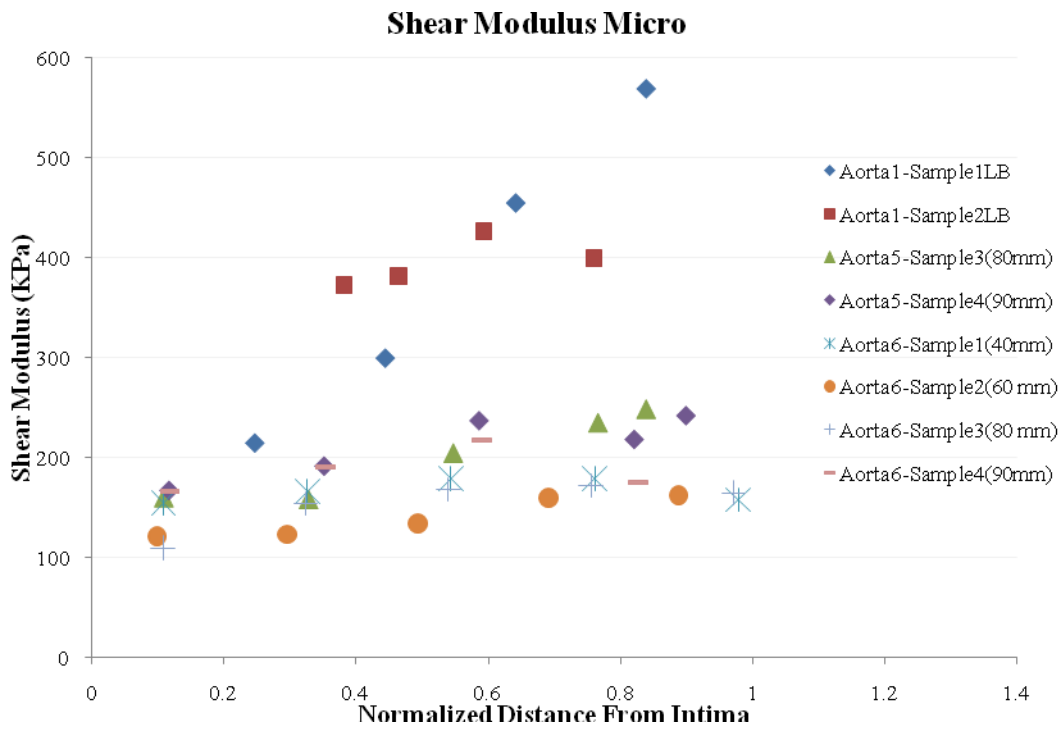


Figure 4.8A: Shear Modulus in the Radial Direction (Micro Indentation).

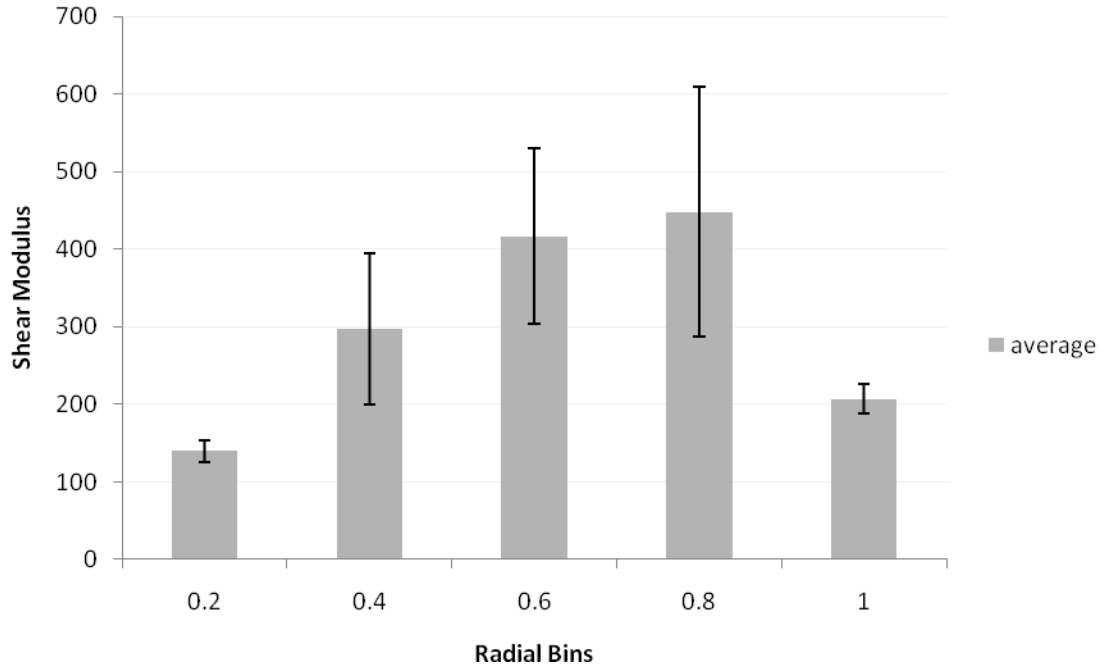


Figure 4.8B: Histogram of the Shear Modulus in the Radial Direction (Micro Indentation).

One idea was that the difference in the material properties in the radial direction may be due to the smooth muscle cells. So for further investigation Sodium Nitro Prusside was applied to one segment of a different aorta (Aorta 4) in order relax the smooth muscle cells and finds its effect on the material properties. The chemical agent relaxed the smooth muscle cells present in the samples (Sample 2, 3, 4). Results of this experiment are shown in Figure 4.9 and Figure 4.10, respectively for lateral and anterior locations. These plots suggest that in the relaxed samples, the shear modulus is mostly homogeneous for the first 60% of the radial thickness confirming that they may contribute to the variation of the instantaneous shear modulus.

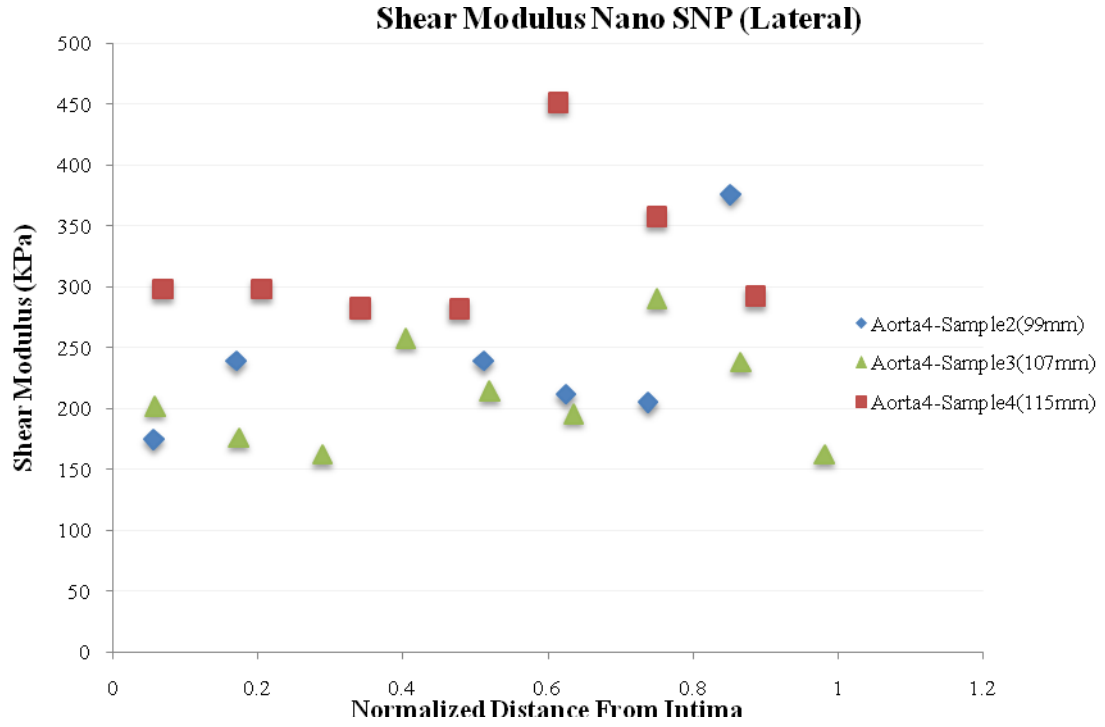


Figure 4.9A: Shear Modulus with SNP (Lateral Nano Indentation).

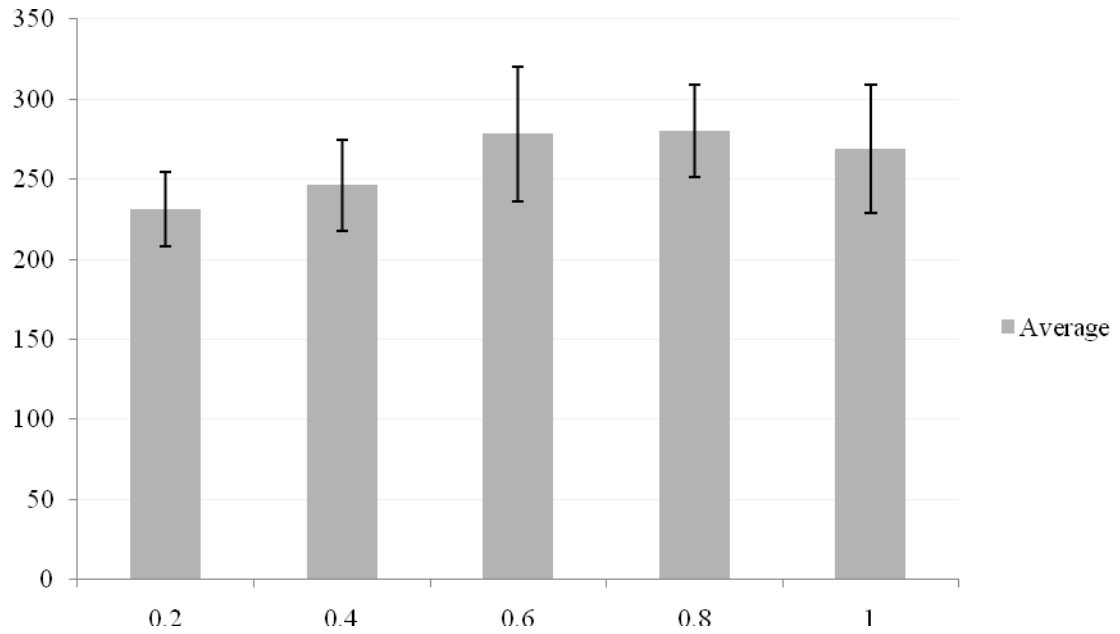


Figure 4.9B: Histogram of the Shear Modulus with SNP (Lateral Nano Indentation).

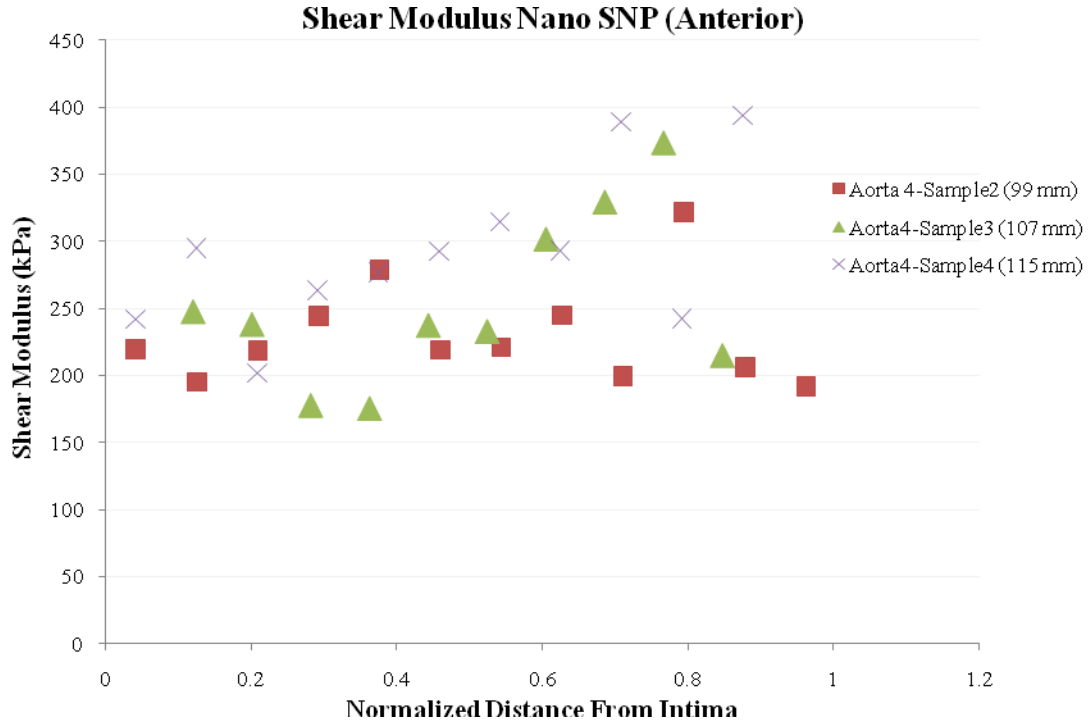


Figure 4.10A: Shear Modulus with SNP (Anterior Nano Indentation).

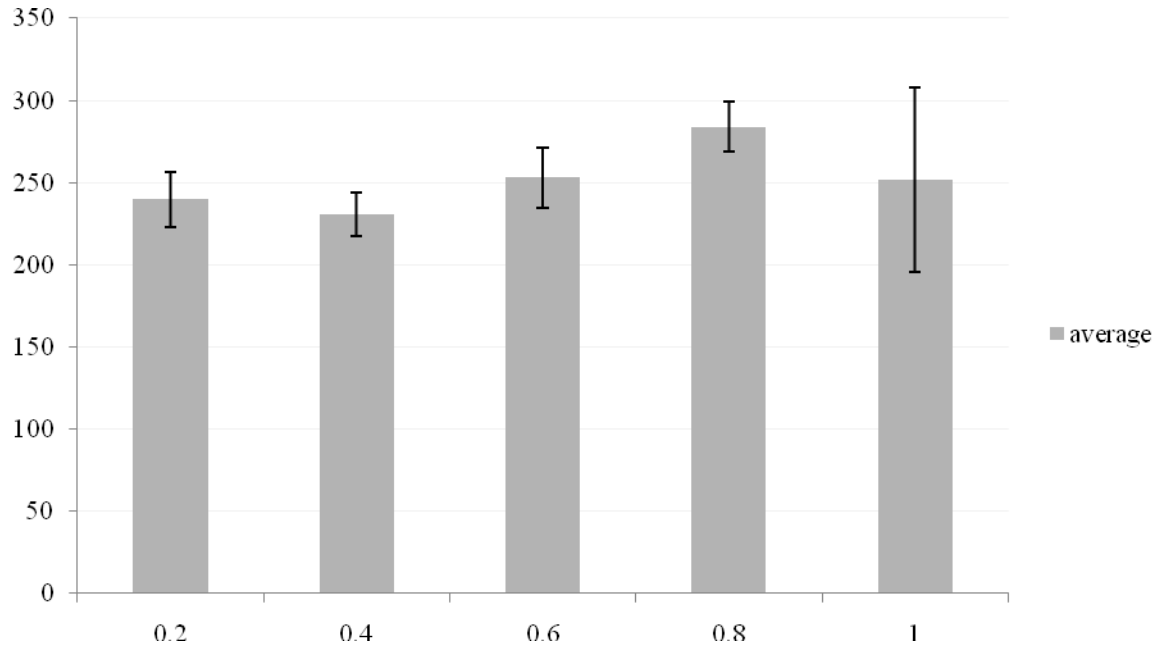


Figure 4.10B: Histogram of the shear modulus with SNP (Anterior Nano Indentation).

Relaxation Functions

The reduced relaxation functions shown in the following charts are a measurement of how much the aortic wall relaxes over time under a constant load.

For a total of 21 tests (Figure 4.11-4.12) analyzed from different samples (S1, S2), no difference was found between micro and nano indentation tests. The aortic tissue relaxes always in the range of 30-40% independent of the longitudinal location and length scale of the sample.

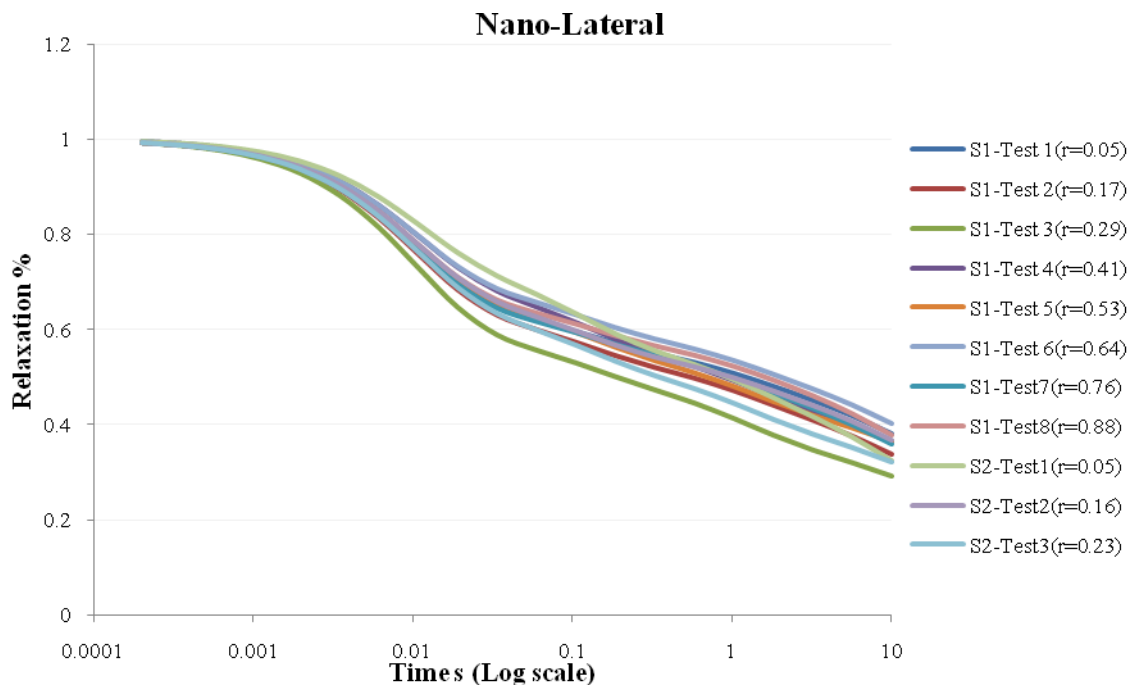


Figure 4.11: Reduced Relaxation Functions from Nano Indentation tests.

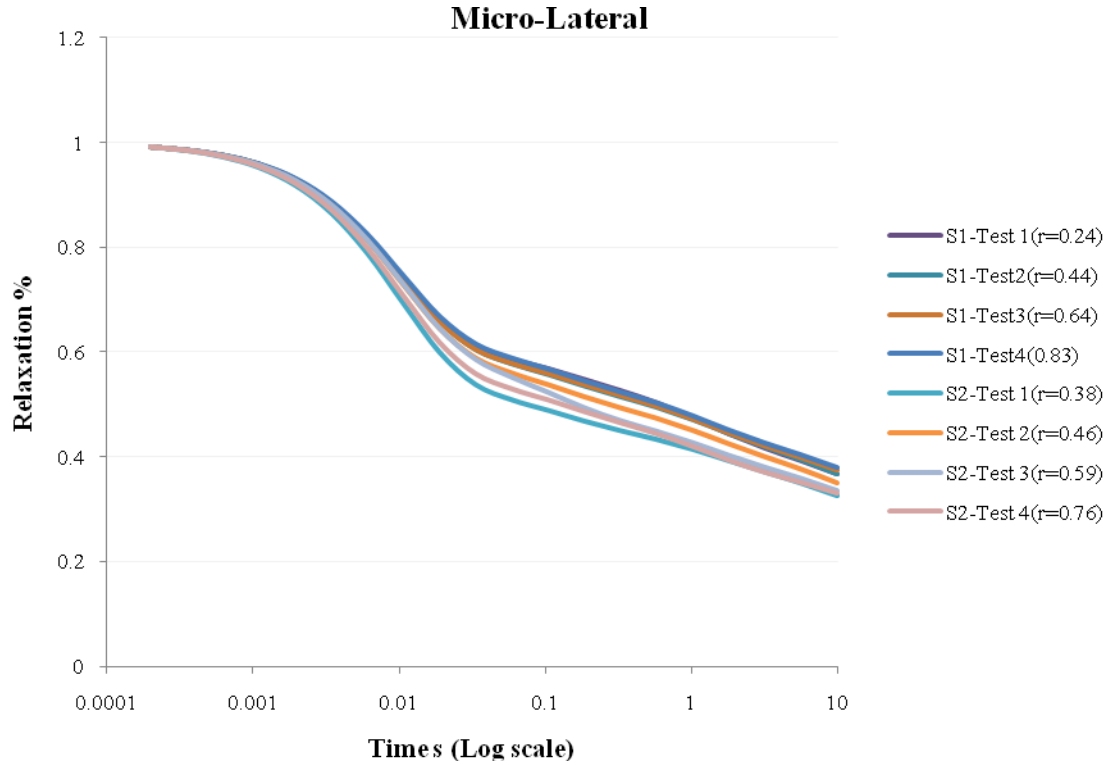


Figure 4.12: Reduced Relaxation Functions from Micro Indentation tests.

As said, during the research process Sodium Nitroprusside was added to a few samples, and curves are shown for nano and micro indentation (Figures 4.13 and 4.14). Here, for nano indentation, the tissue still relaxes approximately 25 to 40 %, while for micro indentation the relaxation percentage is in the order of 40 to 60 %. The test shown have been taken from different samples (S1, S2, S3, S4) not belonging necessarily to the same aortic vessel.

Statistical analysis was performed in order to determine if there is a significant difference between the relaxation functions obtained with different test methods and test agents.

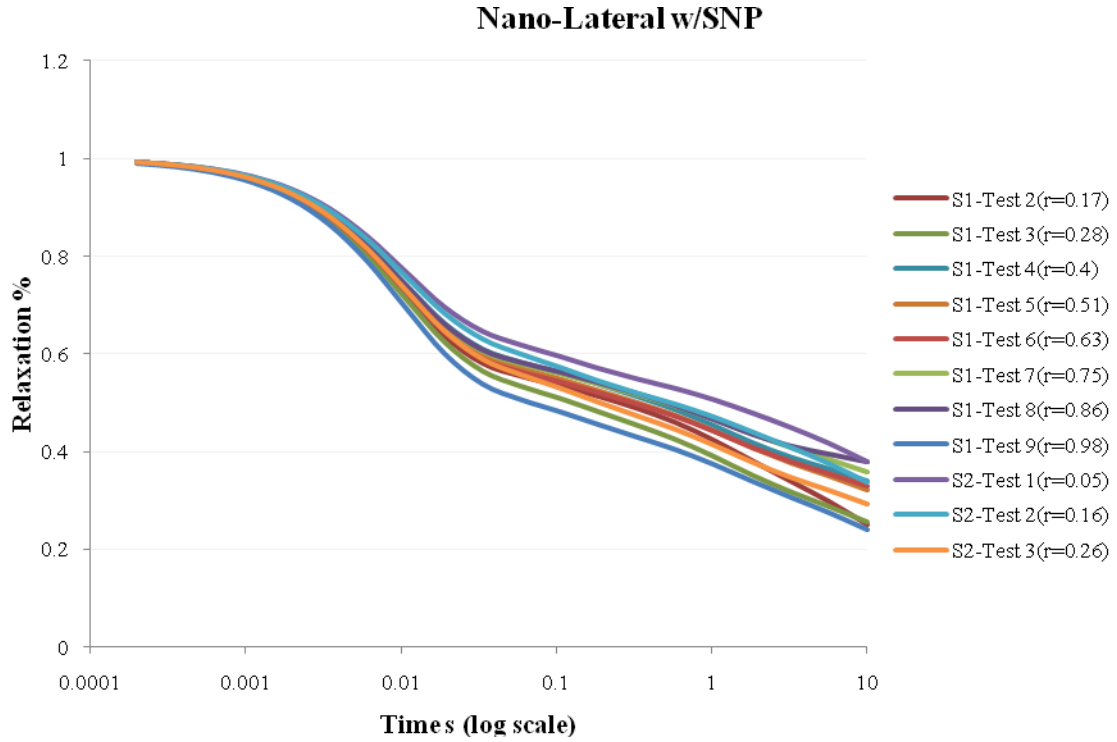


Figure 4.13: Reduced Relaxation Functions Nano Indentation tests w/SNP.

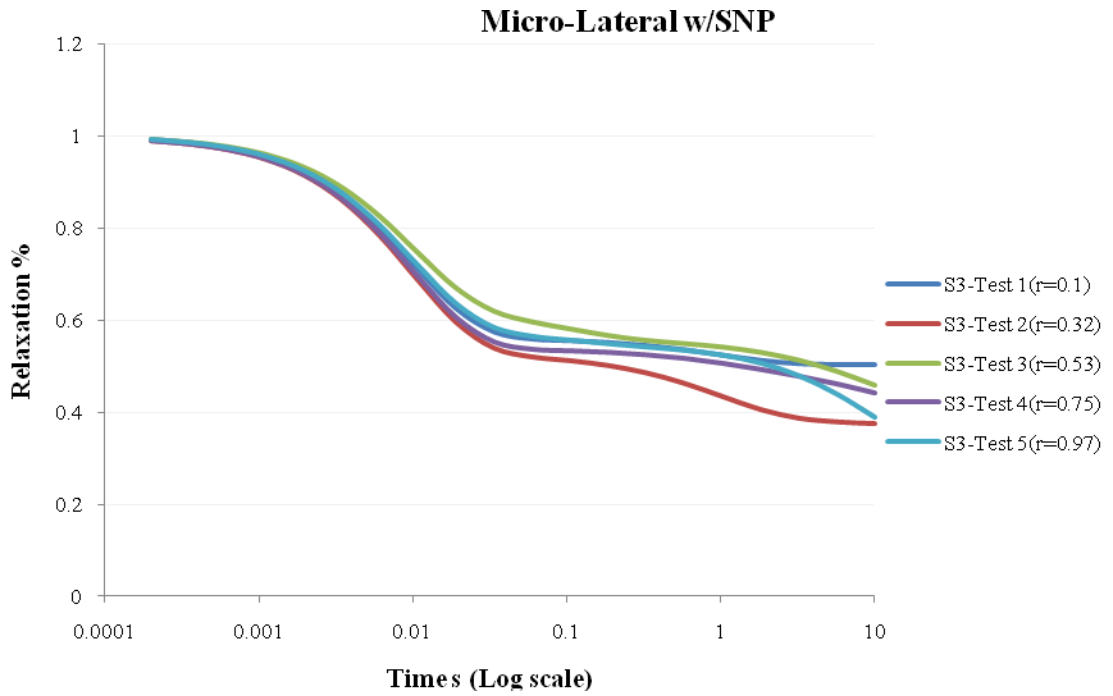


Figure 4.14: Reduced Relaxation Functions Micro Indentation tests w/SNP

Together with the reduced relaxation functions, the trends of the elastic force are approximately similar in both micro and nano indentation data as we can see in the following plot (Figure 4.15). A distinction has been made once again for the samples treated with sodium Nitroprusside and those that were not.

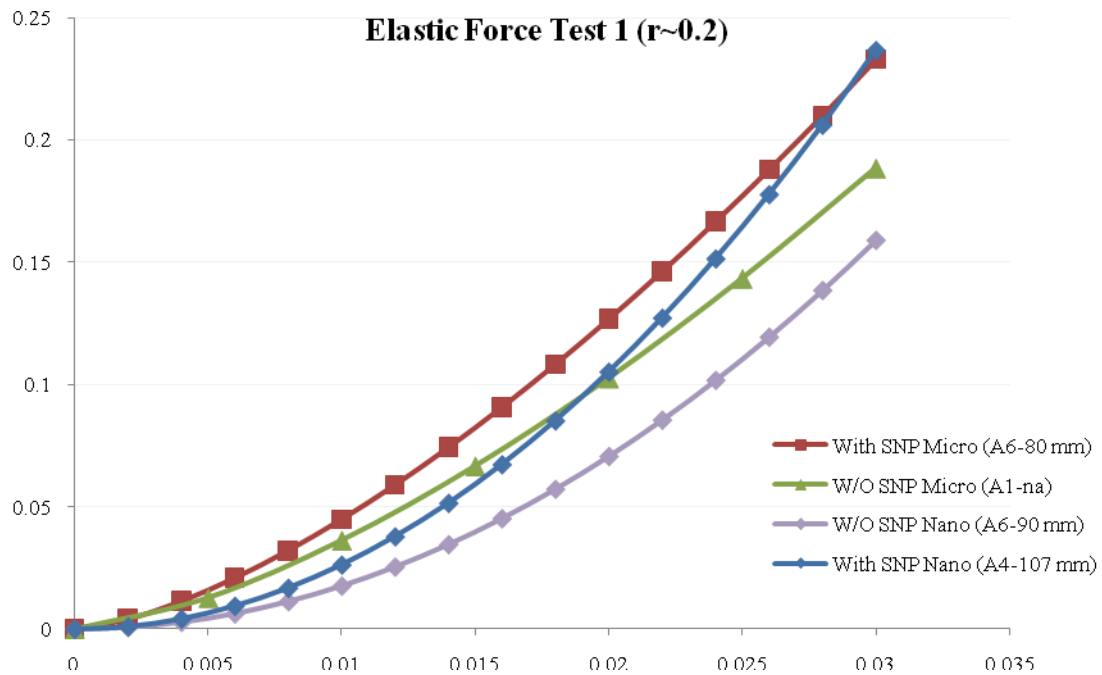


Figure 4.15: Elastic Force Trend

The mechanical nature of fresh aortic tissue is also shown by the values of the reduced relaxation coefficient G_i (Figure 4.16). In particular, G_∞ shows that at most 37% of the material has a purely elastic behavior, stressing the viscoelastic assumption known for biological tissues. The error bars, which represent the standard deviation, show that the variability in each test method and between test methods was relatively small.

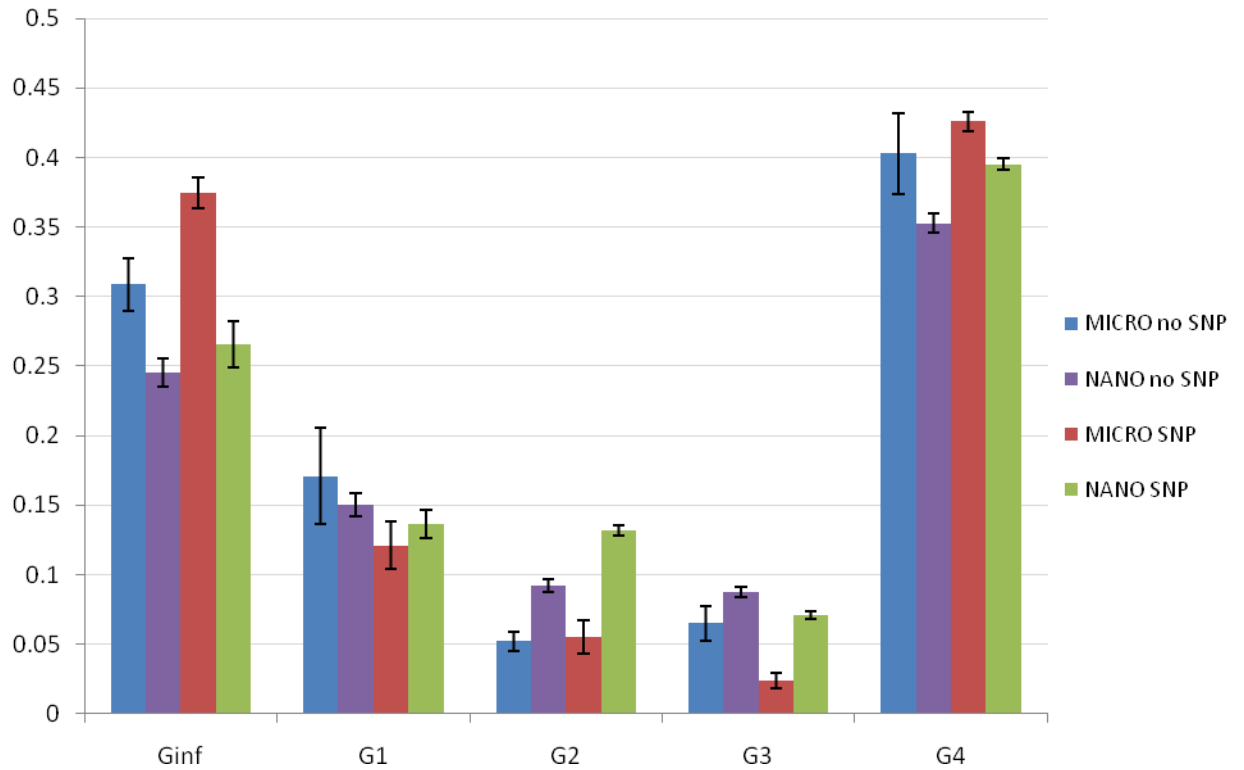


Figure 4.16: Viscoelastic Coefficients Values.

Statistical analysis

In order to establish if the relaxation function has significantly shown differences while tested in different scenarios, t-tests and statistical considerations have been performed.

Relaxation function was analyzed to determine whether or not it depends on:

1. The radial location.
2. The test method (Micro or Nano Indentation).
3. The smooth muscle cell relaxation (SNP).

For the first problem three series of test were analyzed separately and the viscoelastic coefficients were plotted in order to determine if there was a significant difference along the radial direction. The coefficient of determination and the slope was

calculated for the fitting curves found. Table 4.1, 4.2 and Figure 4.17 show how no significant differences were found for the relaxation function in relation to the radial length.

<i>Viscoelastic coefficients</i>	Series 1		Series 2		Series 3	
	R²	Slope	R²	Slope	R²	Slope
G_∞	0.09	0.02	0.01	0.06	0.01	0.01
G1	0.02	0.03	0.01	0.01	0.09	0.06
G2	0.07	0.02	0.05	0.01	0.03	0.03
G3	0.06	0.04	0.02	0.007	0.001	0.006
G4	0.04	0.02	0.03	0.02	0.17	0.1

Table 4.1: R² and slope from curve fitted to Viscoelastic coefficients in the radial direction.

R² is a statistical parameter that gives some information about the goodness of fit of a model. An R² of 1.0 indicates that the regression line perfectly fits the data. The slope close to zero in all the cases demonstrate how the coefficients don't vary while testing in the radial direction. Results from the three series of test were combined while plotted (Fig. 4.17).

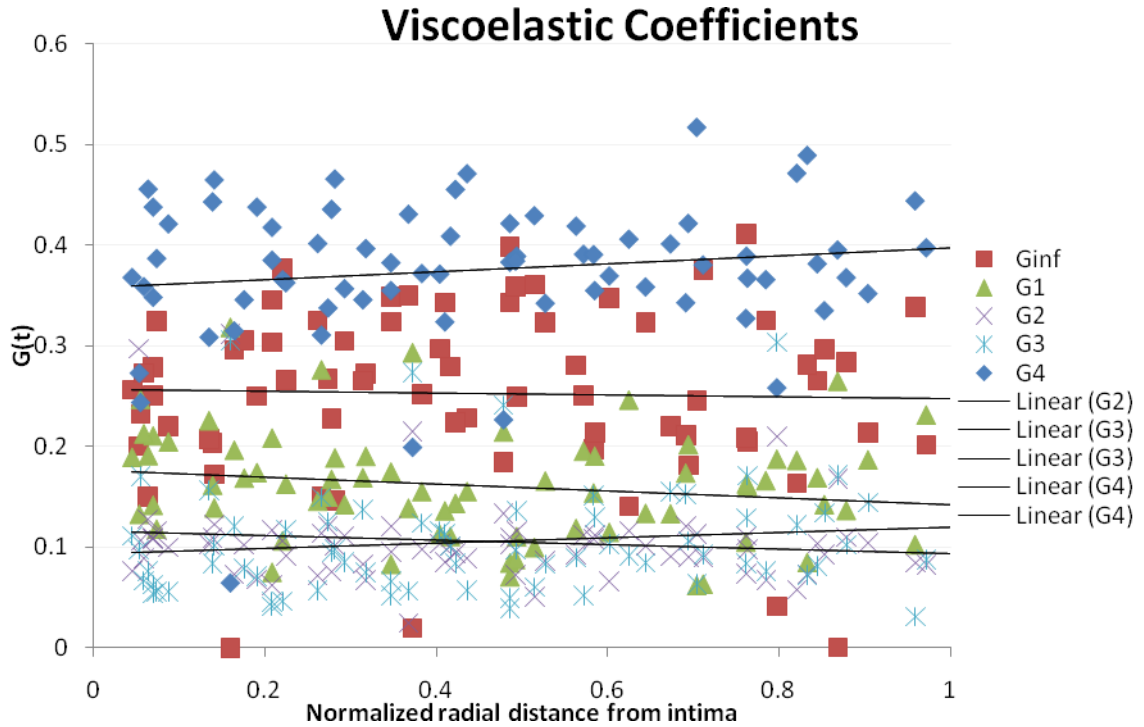


Figure 4.17: Viscoelastic Coefficients in the radial direction.

For the second and third problem t tests were performed comparing the viscoelastic coefficients calculated from:

- Samples subjected to Micro and Nano Indentation
- Samples subjected to Micro Indentation and Micro Indentation with SNP

Table 4.2 and Figure 4.18-4.19 show how no significant differences were found for the relaxation function in relation with the test method or in relation with the SNP agent.

T test results for:	Micro vs Nano <i>p value</i>	Micro with SNP vs Micro <i>p value</i>
G_{∞}	0.07	0.50
$G1$	0.05	0.32
$G2$	0.23	0.51
$G3$	0.0002	0.35
$G4$	0.02	0.54

Table 4.2: T test for viscoelastic coefficients

The t test was used to determine whether two samples are likely to have come from the same two underlying populations that have the same mean. If the result is less than 0.05 they are not likely to be the same.. T tests for $G3$ and $G4$ when compared with test methods (micro and nano indentation) show some significant difference. A possible reason for this can be attributed to the significantly different indenters' sizes.

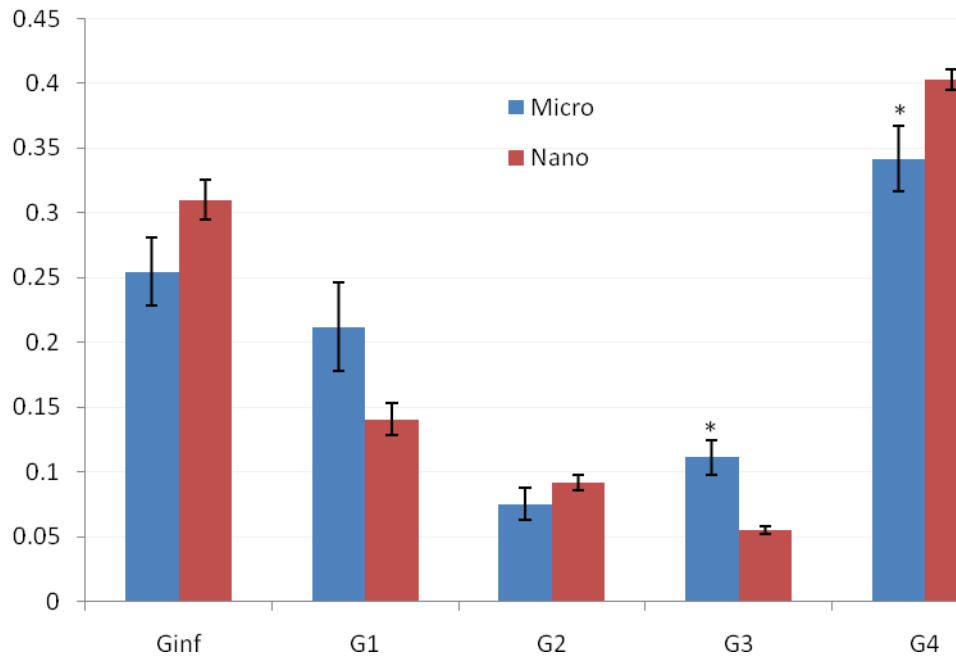


Figure 4.18: Comparison between Viscoelastic Coefficients from Micro and Nano Indentation.

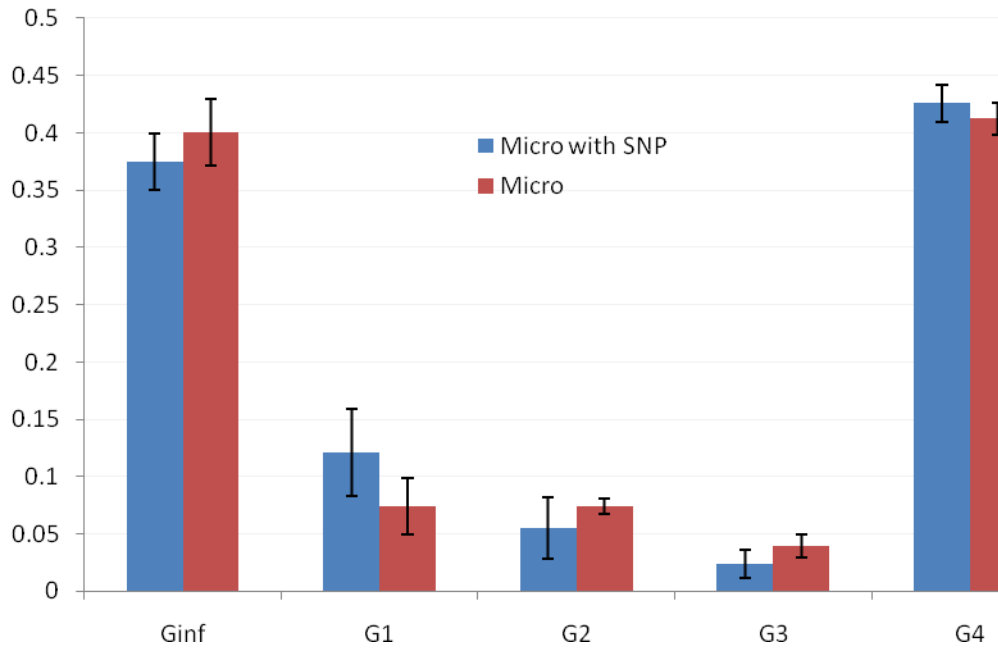


Figure 4.19: Comparison between Viscoelastic Coefficients from Micro Indentation and Micro Indentation with SNP.

Distribution of the smooth muscle cells

Further analysis was then conducted on the distribution of the smooth muscle cells in the aortic wall in order to relate the SNP effects on stiffness with the morphology of the tissue investigated. Pictures were taken at 20X magnification and reconstructed through Photoshop in order to have the entire radial view (Figure 4.20).

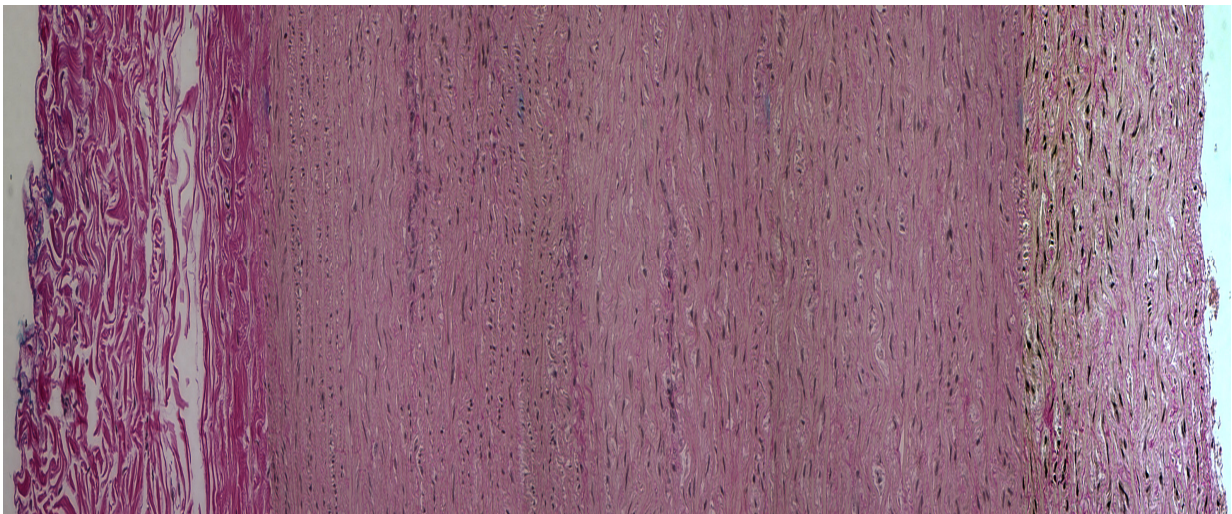


Figure 4.20: Aortic wall reconstruction (20X Mag)

A total of 9 sections derived from 3 samples cut at different longitudinal locations from one descending swine aorta, were analyzed. Sample 1, 2 and 3 were cut respectively 70, 82 and 95 mm under the aortic arch, and the thickness of the sections is approximately 10 μm . Through image analysis, it was possible to discriminate the montage in equal areas and calculate the center point r , determining the distribution of SMC through the aortic wall.

Results show mainly a homogeneous trend up to 60% of the radial thickness, after which there is a clear decrease in number of smooth muscle cells (Figure 4.20A-4.20B).

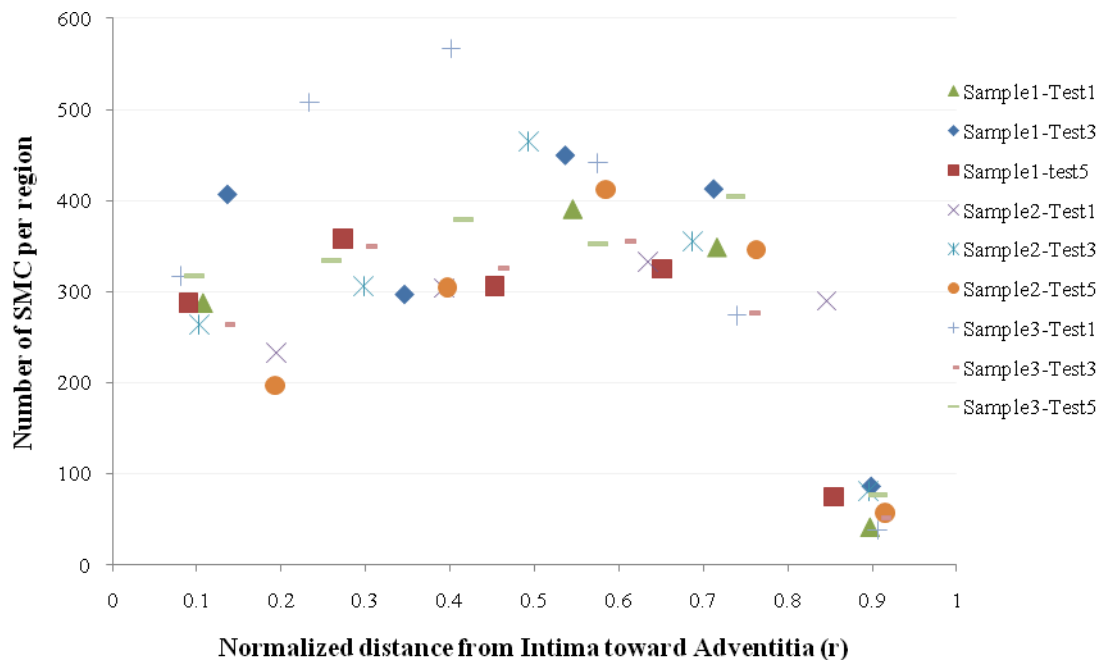


Figure 4.21A: SMC distribution in the radial direction.

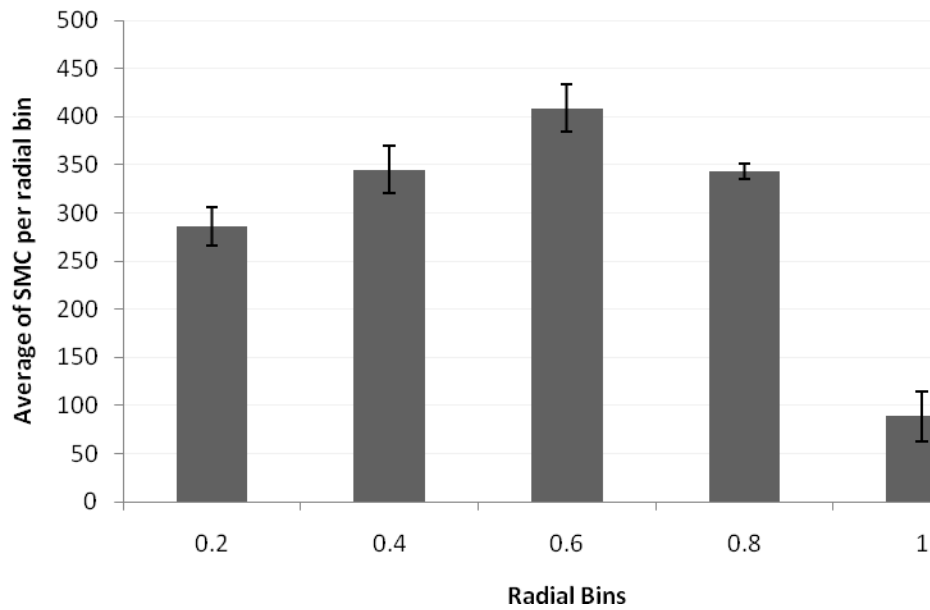


Figure 4.2B: Histogram of the SMC distribution in the radial direction.

CONCLUSIONS

Significant differences were found in shear modulus values showing that a multilayer constitutive model is essential to study the rupture of aorta.

From micro and nano indentation data, the values of aortic shear modulus derived from the instantaneous force data indicate that the material shear modulus is in the range of 150 to 550 kPa, with a linear increment that was found to reach approximately 60% of the radial thickness. The reduced relaxation functions were generally independent of the location and test method.

The inhomogeneous structure composed of mainly collagen, elastin and smooth muscle cells can justify the variability of the stiffness values in the radial and longitudinal direction. The increasing trend found can explain the tear propagation during sudden aortic rupture which is mostly from the intima toward the adventitia. For a given hoop stress, the more compliant region will experience more strain and for a strain based failure will be more prone to failure. The results of Mohan and Melvin (1983) suggest that the failure of aortic wall is strain-based.

The samples treated with the smooth muscle cell relaxer (Sodium Nitro Prusside) do not show such an increasing trend demonstrating how that the variability in the instantaneous shear modulus is partly due to the distribution of the smooth muscle cells. The histology analysis suggests a non uniform distribution of SMC in the aortic wall. More sections will be needed to acquire statistical significance for this observation, but preliminary results show a sharp decrease in number of SMC while moving from media towards adventitia. Smooth muscle cells, in fact, are considered to play an important role in lesion progression (Raghunatha N. RAO, D. *et al.*).

The relation observed between shear modulus and concentration of smooth muscle cells is not exclusive. Collagen and Elastin are the other variables for the constitutive equation and their effect will have to be investigated separately.

CHAPTER 5

DISCUSSION

In a wide range of applications from traumatic injury to stent grafts, finite element (FE) models of the aorta have become an essential tool in designing and optimizing mechanical devices from safety devices for chest injuries to endovascular implants. Current FE models of the aorta assume a homogenous material, but in fact aorta is composed of three major layers: intima, media, and adventitia. Understanding the material properties of these layers is essential in order to study the local mechanisms of deformation, force transmission, and failure. In this study, the material properties of different layers of aorta wall were determined based on a series of micro- and nano-indentation tests. The hypothesis of this work stands in the fact that aorta usually fails in the transverse direction from intima toward adventitia, and therefore the reason why intima fails before the media or adventitia is attributed to the mechanical properties.

The experimental setup was designed to perform indentation testing and the displacement and force were recorded. The force history of the indenter was characterized using a quasi-linear viscoelastic model.

Transverse sections of fresh (2 to 3 hours post-mortem) porcine descending thoracic aorta, 30 to 90 mm below the arch, were tested with two types of indenters: a spherical indenter (0.3 mm diameter) and a conical indenter (200 nm tip curvature), to determine the viscoelastic material properties. The tests were performed mostly on the lateral aorta. The indenter displacement was a ramp and hold with 10 to 30 micron depth,

30 ms ramp time, and 10 s hold time. The force time history of the indenters, measured with ultra-precision force transducers, was characterized using a quasi-linear viscoelastic (QLV) model through a least squares optimization method.

The results showed that the QLV model could sufficiently describe the experimental results. The aorta shear modulus, derived from the instantaneous force function, was in the range of 150 to 450 kPa, with a linear increment that was found to reach approximately 60% of the radial thickness from intima. After this point, the results showed almost constant shear modulus with higher sample to sample variation that was due to the irregular microstructural fiber arrangement in the adventitia compared to the regular circumferential fiber arrangement in the media. Statistical analysis of the models showed that the relaxation function was independent of the radial location, which suggests that the mechanism of damping throughout the aorta wall layers is homogeneous. From the significant differences found in the shear modulus values, it can be concluded that a multilayer QLV constitutive model is essential to study the material properties of aorta. Also, the longitudinal location of the samples with respect to the heart and the length scale (i.e., the difference in size and shape of the indenters) result in differences in the range of the shear modulus.

In some experiments, Sodium Nitroprusside Dehydrate was applied to the samples in order to study the effect of vasodilation, i.e., relaxation of the smooth muscle cells in the material properties. The results showed that the smooth muscle cells contribute to the instantaneous shear modulus but not to the relaxation function. The value of the instantaneous shear modulus was more uniform in the radial direction in the samples treated with SNP. The smooth muscle cells can be considered as elastic elements that act in parallel to the collagen fibers and elastin lamellae and reduce the overall stiffness particularly in the regions in inner media where their concentration is higher. More studies are needed to quantify the variability in the distribution of collagen

fibers and elastin lamellae in the radial and circumferential directions to be able to construct a more comprehensive micro-structure-based constitutive model for the aorta wall.

BIBLIOGRAPHY

Bass CR, Darvish K, Bush B, Crandall JR, Srinivasan SC, Tribble C, Fiser S, Tournet L, Evans JC, Patrie J, Wang C. (2001). "Material Properties for Modeling Traumatic Aortic Rupture." *Stapp Car Crash Journal* 45: 143-60.

Bec, Sandrine, Andre Tonck and Jean-Luc Loubet. (1994). "Indentation at the Nanometer Scale on Ultra Thin Films of Diamond-Like Carbon." *Proceedings of the 1994 Fall Meeting of MRS.*

Brossollet, Louis J., and Raymond P. Vito. (1995). "An Alternate Formulation of Blood Vessel Mechanics and the Meaning of the in Vivo Property." *Journal of Biomechanics* 28.6 : 679-87.

Cavanaugh J M, Walilko T J, Malhotra A, Zhu Y, King A. (1992). "Biomechanical Response and Injury Tolerance of the Thorax in Twelve Sled Side Impacts." *SAE Paper No.902307.*

Cheng, GC, et al. (1993). "Distribution of Circumferential Stress in Ruptured and Stable Atherosclerotic Lesions. A Structural Analysis with Histopathological Correlation." *Circulation* 87.4: 1179-87.

Cheung, J. B., and C. C. Hsiao. (1972). "Nonlinear Anisotropic Viscoelastic Stresses in Blood Vessels." *Journal of Biomechanics*, 5.6 (1972): 607-19.

Choserot, Christophe, et al. (2005). "Experimental Comparison between Autofluorescence Spectra of Constrained Fresh and Cryopreserved Arteries." *Clinical Hemorheology & Microcirculation* 33.3: 235-42.

Darvish K. , Lobovsky L. , Lee S. (2004). "Analysis and Modeling of Aortic Tissue Material Properties." *ASME International Mechanical Engineering Congress.*

Dellman, Horst-Dieter, Brown. Esther M. (1981). Textbook of Veterinary Histology. Second ed.

Dorfmann, A., and R. W. Ogden. (2003). "A Pseudo-Elastic Model for Loading, Partial Unloading and Reloading of Particle-Reinforced Rubber." *International Journal of Solids and Structures* 40.11: 2699-714.

Etave, Frédérique, et al. (2001) "Mechanical Properties of Coronary Stents Determined by using Finite Element Analysis." *Journal of Biomechanics* 34.8: 1065-75.

Fattori R. , Celletti F. , Bertaccini P. , Galli R. , Pacini D. , Pierangeli A. , Gavelli G. (1994). "Delayed Surgery of Traumatic Aortic Rupture." *Circulation*: 94:2865-2870.

Fawcett, Don W. (1994). A Textbook of Histology. Twelfth ed., Chapman and Hall, New York.

Findley, W. N., Lai, J. S., and Onaran, K. (1976) "Creep and Relaxation of Nonlinear Viscoelastic Materials", North-Holland Publishing Company.

Fung, Y. C. (1993). "Mechanical Properties of Living Tissues." *Biomechanics*. second ed. Springer.

Gordon Aylward and Tristan Findlay, ed. *SI Chemical Data Book* (4th Ed.).

H. Lu, B. Wang, J. Ma, G. Huang and H. Viswanathan (2003). "Measurement of Creep Compliance of Solid".

Hardy WN, Shah CS, Mason MJ, Kopacz JM, Yang KH, King AI, Van Ee CA, Bishop JL, Banglmaier RF, Bey MJ, Morgan RM, Digges KH. "Mechanisms of Traumatic Rupture of the Aorta and Associated Peri-Isthmic Motion and Deformation."

He, C.M., Roach, M.R. "The Composition and Mechanical Properties of Abdominal Aortic Aneurysms." *Journal of Vascular Surgery*.

Holzapfel, G. A., T. C. Gasser, and M. Stadler. (2002). "A Structural Model for the Viscoelastic Behavior of Arterial Walls: Continuum Formulation and Finite Element Analysis." *European Journal of Mechanics - A/Solids*, 21.3: 441-63.

J. Xavier-Neto, E. M. Krieger "Viscoelastic Behavior of "in Situ" Aortic Wall during Hemorrhagic Hypotension."

Jacques, Ohayon¹, et al. "A Three-Dimensional Finite Element Analysis of Stress Distribution in a Coronary Atherosclerotic Plaque: in-Vivo Prediction of Plaque Rupture Location."

Jonathan P. Vande Geest, Michael S. Sacks, David A. Vorp. "Age Dependency of the Biaxial Biomechanical Behavior of Human Abdominal Aorta."

Kalita, P., and R. Schaefer. (2008). "Mechanical Models of Artery Walls". Archives of Computational Methods in Engineering 15.1: 1-36.

Katyal D., McLellan B.A., Brenneman F.D., Boulanger B.R., Sharkey P.W., Waddell J.P. (1997). "Lateral Impact Motor Vehicle Collisions: Significant Cause of Blunt Traumatic Rupture of the Thoracic Aorta." J. Trauma: 42(5):769-772.

Kermouche, G., J. L. Loubet, and J. M. Bergheau. (2008). "Extraction of stress-strain Curves of elastic-viscoplastic Solids using conical/pyramidal Indentation Testing with Application to Polymers." Mechanics of Materials, 40.4-5: 271-83.

Koay EJ, Shieh AC, Athanasiou KA. (2003). "Creep Indentation of Single Cells." Journal of Biomechanical Engineering-Transactions of the Asme: 125(3):334-41.

Lee SH, Kent R. (2007). "Blood Flow and Fluid-Structure Interactions in the Human Aorta during Traumatic Rupture Conditions." (Stapp Car Crash J. 51:211-33.)

Lu, H. , Wang, B. , Ma, J., Hiang, G. and Viswanathan, H. (2003). "Measurement of Creep Compliance of Solid Polymers by Nanoindentation." Mechanics of Time-Dependent Materials 7: 189-207.

Matsumoto, Takeo, et al. (2004). "Residual Stress and Strain in the Lamellar Unit of the Porcine Aorta: Experiment and Analysis." Journal of Biomechanics 37.6: 807-15.

McVeigh, G. E., P. K. Hamilton, and D. R. Morgan. (2002). "Evaluation of Mechanical Arterial Properties: Clinical, Experimental and Therapeutic Aspects." Clinical Science 102.1: 51-67.

Ming, Zhang, Y. P. Zheng, and Arthur F. T. Mak. (1997). "Estimating the Effective Young's Modulus of Soft Tissues from Indentation Tests--Nonlinear Finite Element Analysis of Effects of Friction and Large Deformation." Medical Engineering & Physics, 19.6: 512-7.

Mirsky, I. (1973). "Ventricular and Arterial Wall Stresses Based on Large Deformation Analyses." Biophysical Journal 13.11: 1141-59.

Mohan, Dinesh, Melvin, John W. (1983). "Failure Properties of Passive Human Aortic Tissue. II—Biaxial Tension Tests." Journal of Biomechanics 16.1: 31-7.

Mohan, Dinesh, and John W. Melvin. (1982). "Failure Properties of Passive Human Aortic Tissue. I—Uniaxial Tension Tests." Journal of Biomechanics 15.11: 887-93.

Moore, James E., et al. (1994). "Fluid Wall Shear Stress Measurements in a Model of the Human Abdominal Aorta: Oscillatory Behavior and Relationship to Atherosclerosis." *Atherosclerosis* 110.2: 225-40.

O'Connell, Mary K., et al. (2008). "The Three-Dimensional Micro- and Nanostructure of the Aortic Medial Lamellar Unit Measured using 3D Confocal and Electron Microscopy Imaging." *Matrix Biology*, 27.3: 171-81.

Oliver, W. C., and G. M. Pharr. (2004). "Measurement of Hardness and Elastic Modulus by Instrumented Indentation: Advances in Understanding and Refinements to Methodology." *Journal of Materials Research* 19.1: 3-20.

Parmley LF, Mattingly TW, Manion WC, et al. (1958). "Nonpenetrating Traumatic Injury of the Aorta." (*Circulation*. 17:1086-1101).

Patel, Doli J., Joseph S. Janicki, and Thomas E. Carew. (1969). "Static Anisotropic Elastic Properties of the Aorta in Living Dogs." *Circulation Research* 25.6: 765-79.

Pearson, Richard, et al. (2008). "Regional Wall Mechanics and Blunt Traumatic Aortic Rupture at the Isthmus." *European Journal of Cardio-Thoracic Surgery* 34.3: 616-22.

Raghavan, M. L., and David A. Vorp. (2000). "Toward a Biomechanical Tool to Evaluate Rupture Potential of Abdominal Aortic Aneurysm: Identification of a Finite Strain Constitutive Model and Evaluation of its Applicability." *Journal of Biomechanics*, 33.4: 475-82.

Richens, D., et al. (2003). "Rupture of the Aorta Following Road Traffic Accidents in the United Kingdom 1992–1999. the Results of the Co-Operative Crash Injury Study." *European Journal of Cardio-Thoracic Surgery*, 23.2: 143-8.

Sahay, K. B., and Dinesh Mohan. (1984). "Strain Energy Characterisation of Human Aortic Tissue in Uniaxial Tension." *Journal of Biomechanics*, 17.11: 877.

Serafini-Fracassini, A., et al. (1976). "The Macromolecular Organization of the Elastin Fibril." *Journal of Molecular Biology* 100.1: 73-84.

Shahcheraghi, N., et al. (2002). "Unsteady and Three-Dimensional Simulation of Blood Flow in the Human Aortic Arch." *Journal of Biomechanical Engineering-Transactions of the Asme* 124.4: 378-87.

Shin-ichiro Katsuda, et al. (2004). "Change in the Static Rheological Properties of the Aorta in Kurosawa and Kusanagi-Hypercholesterolemic Rabbits with Progress of Atherosclerosis." *Physiological Measurement*.

Sneddon, I. N. (1965). "The Relation between Load and Penetration in the Problem for a Punch of Arbitrary Profile." *International Journal of Engineering Science*, 3, 47-57.

Sokolis, D. P. (2007). "Passive Mechanical Properties and Structure of the Aorta: Segmental Analysis." *Acta Physiologica* 190.4: 277-89.

Spina, M., et al. (1983). "Age-Related-Changes in composition and mechanical-properties of the tunica media of the upper thoracic human aorta." *Arteriosclerosis* 3.1: 64-76.

Stemper, Brian D., Narayan Yoganandan, and Frank A. Pintar. (2007). "Mechanics of Arterial Subfailure with Increasing Loading Rate." *Journal of Biomechanics*, 40.8: 1806-12.

Tanaka, Toshiyuki T., and Yuan-Cheng Fung. (1974). "Elastic and Inelastic Properties of the Canine Aorta and their Variation Along the Aortic Tree." *Journal of Biomechanics*, 7.4: 357-70.

Vande Geest, Jonathan P., Elena S. Di Martino, and David A. Vorp. (2004). "An Analysis of the Complete Strain Field within Flexercell™ Membranes." *Journal of Biomechanics*, 37.12: 1923-8.

Vande Geest, Jonathan P., Michael S. Sacks, and David A. Vorp. (2006). "The Effects of Aneurysm on the Biaxial Mechanical Behavior of Human Abdominal Aorta." *Journal of Biomechanics*, 39.7: 1324-34.

Vito R.P., Dixon S.A. (2003). "Blood Vessel Constitutive Models " *Annu. Rev. Biomed. Eng.* 5:413-39.

Vorp, David A. (2007). "Biomechanics of Abdominal Aortic Aneurysm." *Journal of Biomechanics*, 40.9: 1887-902.

Wang, James H. -C, et al. (2001). "Specificity of Endothelial Cell Reorientation in Response to Cyclic Mechanical Stretching." *Journal of Biomechanics*, 34.12: 1563-72.

Wei, Pal Jen, and Jen Fin Lin. (2008). "Determination for Elasticity and Plasticity from Time-Dependent Nanoindentations." *Materials Science and Engineering: A*, 496.1-2: 90-7.

Weiss, Leon. (1998). *Cell and Tissue Biology, A Textbook of Histology*. Sixth ed.

Y. C. Fung. (1993). "The Meaning of the Constitutive Equation." *Biomechanics*. Ed. Springer.

Zhao, Aihong, et al. (2008). "Blunt Trauma and Acute Aortic Syndrome: A Three-Layer Finite-Element Model of the Aortic Wall." *European Journal of Cardio-Thoracic Surgery*, 34.3: 623-9.

Raghunatha N. Raoa, et al. (1999). "Intimal Thickness and Layering, and Smooth Muscle Cell Phenotypes in Aorta of Youth." *Pathobiology* 2000;68:18-28

APPENDICES

APPENDIX A

Isthmus region - Anatomy

The isthmic region (Figure A.1) lies in between the aortic arch and the descending aorta, and 94% of all TAR related to car accidents occur within this region {{74 Amanda Law; }}, and 93% of the tears are complete.

The mechanism of TAR and associated peri-isthmic motion and deformation has been studied widely and in particular at the University of Wayne: eight un-embalmed human cadavers were tested using different dynamic blunt loading modes and the peri-isthmic region was monitored by radiopaque markers. Results show that longitudinal stretch of the aorta is a principal component for injury.

The stretch of aorta was generated by thoracic deformation, which is required for injury to occur. The peri-isthmic region is subject to the greatest strain compared to the other regions of the vessel. Proof of this statement was movement that the peri-isthmic experienced during the crash test; the isthmus moved dorsocranially during frontal impact and submarining loading modes. The aortic isthmus moved medially and anteriorly during impact to the left side (Hardy WN, Shah CS et. al).

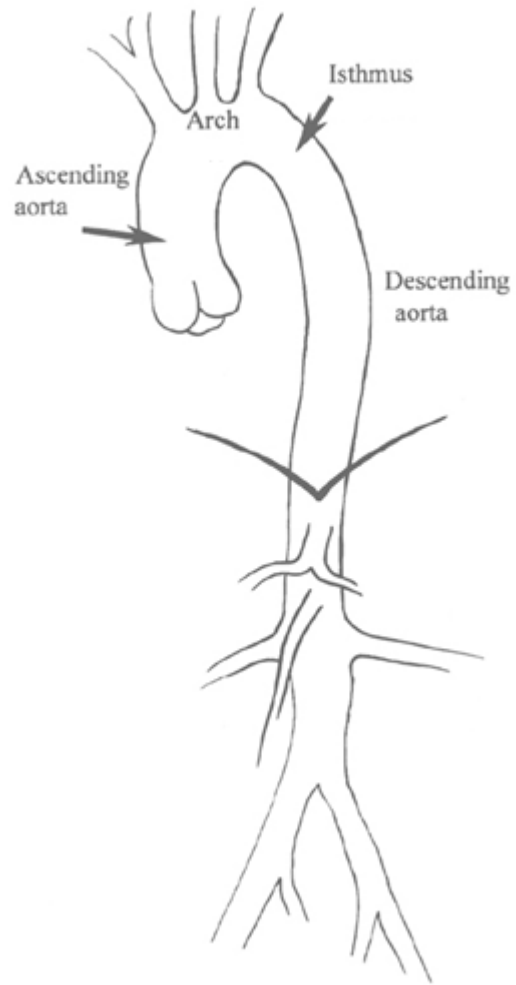


Figure A.1: Aorta's regions

<http://www.ivasbr.com.br/03-02-03/03-02-03-197/fig02.jpg>

APPENDIX B

Sodium Nitroprusside Dihydrate Composition

Sodium Nitroprusside Dihydrate is a strong vasodilator and it is often administered to hypertensive patients; the chemical compound has the following formula



This red solid anion dissolves in water (0.01% is insoluble) and in saline solution, as proved during the fourth series of experiments conducted in the present study.

Sodium nitroprusside is disodium pentacyanonitrosylferrate(2-) dihydrate is a inorganic hypotensive agent whose structural formula is

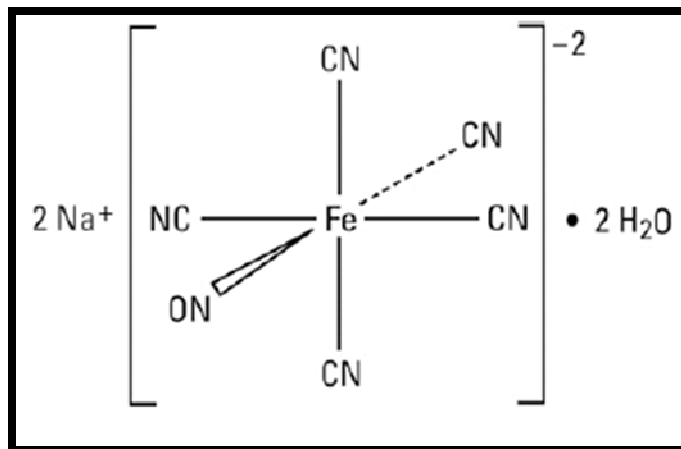


Figure B.1: Sodium Nitroprusside Structural Formula

(<http://www.rxlist.com/nitropruss-drug.htm>)

Its molecular weight is 297.95; the dosage necessary to relax the smooth muscle cells present in the samples for the present study was established to be M.

Sodium NitroPrusside Calculation			
M _r	297.95	g	
M=N/V	1.00E-05	M	
V	0.36	L	
N	3.60E-06	moles	
x	1.07E-03	g	
	0.00107	g	

Table B.1: Sodium Nitroprusside Calculation

The function of this compound in the present experiments is to create local microvascular vasodilatation. Nitric oxide (NO) liberated from the Sodium NitroPrusside diffuses into the vascular smooth muscle cells causing relaxation and subsequent vasodilatation.

In clinical settings this compound can be used to reduce total peripheral resistance as well as venous return, decreasing preload and afterload; if the cardiac output is normal, the effect is blood pressure reduction.

APPENDIX C

Fundamentals of Viscoelasticity

If a body is suddenly strained and the strain is kept constant, the corresponding stress induced in the body decreases in time; this feature is called relaxation. This phenomenon is found especially in biological materials and together with creep and hysteresis the material can be defined as viscoelastic (Fung YC. 1993).

Mechanical models are often used to represent the viscoelastic behavior of viscoelastic materials; in Figure C.1 are shown the fundamental mechanical models called, from left to right, Maxwell model, Voigt model and Kelvin or standard linear model.

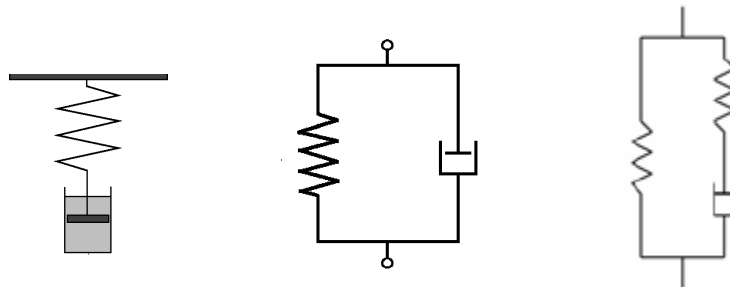


Figure C.1: Three mechanical models of viscoelastic material

Aortas relaxation function can be associated closely to the standard linear model, as we can see in Figure C.2, where the strain applied is given from the displacement and the force relaxes throughout the 10 seconds recorded.

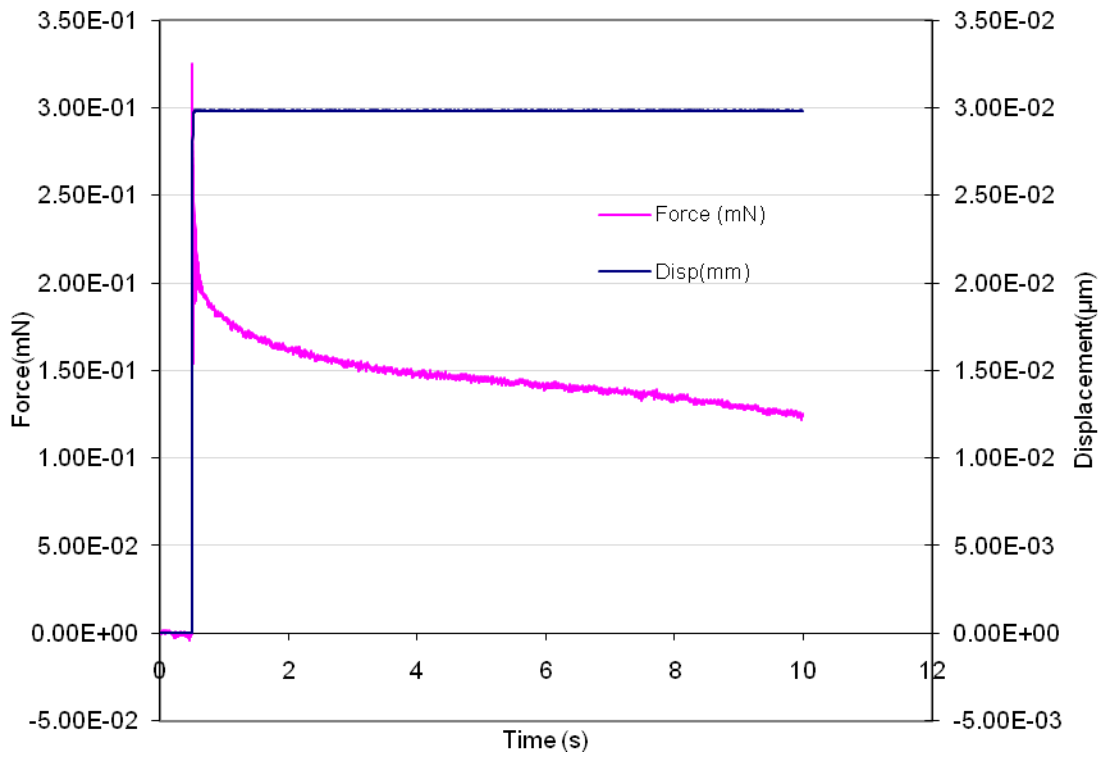


Figure C.2: Relaxation Function (Force) and Deformation (Displacement)

More general models can be built by combining or adding more elements to the three models listed to better represent the physical phenomena investigated.

APPENDIX D

Van Gieson Staining Protocol

Van Gieson Stain differentiates collagen from other connective tissue. The protocol and solutions utilized for this procedure are the following:

- Van Gieson Solution
 - Weigert's Iron Hematoxylin A
 - Weigert's Iron Hematoxylin B
-
1. Deparaffinize and hydrate to distilled water
 2. Soak in Weigert's Working Hematoxylin 10 min
 - a. Weigert's Working Solution is prepared by mixing equal parts of Weigert's Iron Hematoxylin A and Weigert's Iron Hematoxylin B
 3. Wash in distilled water
 4. Soak in Van Gieson Solution 1 to 3 min
 5. Dehydrate in 95% alcohol, absolute alcohol, two changes each.
 6. Clear in two changes Xylene
 7. Mount with Permount or DPX.

Stain Results:

Collagen	<i>Red</i>
Smooth and striated muscle	<i>Yellow to Brown</i>
Nuclei	<i>Blue to Black</i>

Van Gieson. New York Med, 1889.